Journal of Sedimentary Research

Journal of Sedimentary Research, 2020, v. 90, 1156–1174
Research Article
DOI: http://dx.doi.org/10.2110/jsr.2020.58

CONTROLS ON DOLOMITIZATION IN EXTENSIONAL BASINS: AN EXAMPLE FROM THE DERBYSHIRE PLATFORM, U.K.

CATHERINE BREISLIN,*[1] STEPHEN CROWLEY,[2] VANESSA J. BANKS,[3] JIM D. MARSHALL,[2] IAN L. MILLAR,[3] JAMES B. RIDING,[3] AND CATHY HOLLIS[1]

[1]*Department of Earth and Environmental Science, University of Manchester*
[2]*Jane Herdman Laboratories, University of LIverpool*
[3]*British Geological Survey*

ABSTRACT: **Fault-controlled dolomitization has been documented in Lower Carboniferous (Viséan) platform carbonates at various localities in the Pennine Basin and North Wales. The largest of these dolomite bodies (approx. 60 km^2) occurs on the Derbyshire Platform, on the southern margin of the Pennine Basin. This study tests the hypothesis that dolomitization occurred at this locality during deposition, platform drowning, and the earliest stages of burial, coincident with the transition from a late syn-rift to post-rift regime. It also assesses the importance of syn-rift volcanism on dolomitization. Planar, fabric-retentive dolomite with single-phase (i.e., low temperature) fluid inclusions occurs along NW–SE and E–W oriented faults, and in platform margin facies and in proximity to the Masson Hill Volcanic Complex. Oxygen isotope data are consistent with dolomitization from seawater, but slightly depleted $\delta^{13}C$ values reflect mixing with magmatic fluids. Volcanic activity is likely to have produced a thermal drive for fluid circulation on the platform margin, and post-depositional alteration of basalts by CO_2-rich fluids could have led to alteration of olivine and release of magnesium to convecting seawater. Consequently, the large volume of dolostone on the southern margin of the Derbyshire Platform is attributed to the increased geothermal gradient and a localized increase in the Mg/Ca ratio of dolomitizing fluids at this locality, compared to elsewhere in the Pennine Basin. The results suggest that syn-rift carbonate platforms in volcanically active areas of rift basins have a greater potential for dolomitization from seawater than non-volcanic platforms in the same basin.**

INTRODUCTION

Geothermal convection of seawater can lead to dolomitization on carbonate-platform margins (e.g., Wilson et al. 2001; Whitaker and Xiao 2010). Recently, interest has grown in the relationship between dolomitization and volcanism. In particular, fault-controlled dolomitization has been related to syn-rift igneous activity on the Latemar platform (e.g., Zheng 1990; Carmichael and Ferry 2008; Blomme et al. 2017; Jacquemyn et al. 2017) the Levant region (Nader et al. 2004), and West Point Formation, Quebec (Lavoie et al. 2010). However, the contribution of syn-rift volcanic activity on dolomitization is still uncertain. For example, although heat flow is increased during volcanism, facilitating geothermal convection, submarine extrusion of lava can result in a net removal of magnesium from seawater through the formation of chlorite (Reed and Palandri 2006). Recent geochemical modeling by Robertson et al. (2019), however, has shown that ultramafic carbonation can substantially increase the Mg/Ca ratio of fluids, but the extent to which this increases dolomitization potential in nature has not been evaluated.

In the Pennine Basin and North Wales, UK, fault-controlled dolostone bodies are developed on the margins of Mississippian carbonate platforms that grew on the rotated footwalls of normal faults and a basement of lower Paleozoic metasediments (Fig. 1) that were reactivated during Carboniferous extension and basin inversion during the Variscan Orogeny (Fraser and Gawthorpe 2003). Dolostone is also observed in basinal and platform carbonate sediments (Gawthorpe 1987; Hollis and Walkden 2012). Although the size and shape of these geobodies have been consistently described in the literature (Fowles 1987; Gawthorpe 1987; Ford 2002; Bouch et al. 2004; Hollis and Walkden 2012; Frazer 2014; Frazer et al. 2014; Juerges et al. 2016), numerous dolomitization models have been proposed to explain their formation. Most of these dolomite bodies have been interpreted to have formed from basinal brines, expelled during post-rift thermal subsidence and basin inversion (e.g., Schofield and Adams 1986; Gawthorpe 1987; Bouch et al. 2004; Hollis and Walkden 2012; Frazer et al. 2014; Juerges et al. 2016).

The Derbyshire Platform, located at the southern margin of the Pennine Basin (Figs. 1, 2), comprises Lower Carboniferous (Viséan) platform carbonates deposited in a back-arc extensional regime (Fraser and Gawthorpe 2003). The Derbyshire Platform hosts the largest volume of dolostone of all the platforms in the Pennine Basin, estimated by Ford (2002) to be 50 km^2 of dolostone, compared to approx. 8 km^2 on the North Wales Platform (Juerges et al. 2016) and approx. 20 km^2 on the Askrigg Platform and Craven Basin (Hollis and Walkden 2012). Despite its volume, however, there is still a lack of consensus as to the mechanism that formed this large dolostone geobody. Fowles (1987) proposed dolomitization

* Present Address: Badley Ashton and Associates, Winceby House, Winceby, Horncastle, Lincolnshire LN9 6BP, U.K.

Published Online: September 2020
 1527-1404/20/090-1156

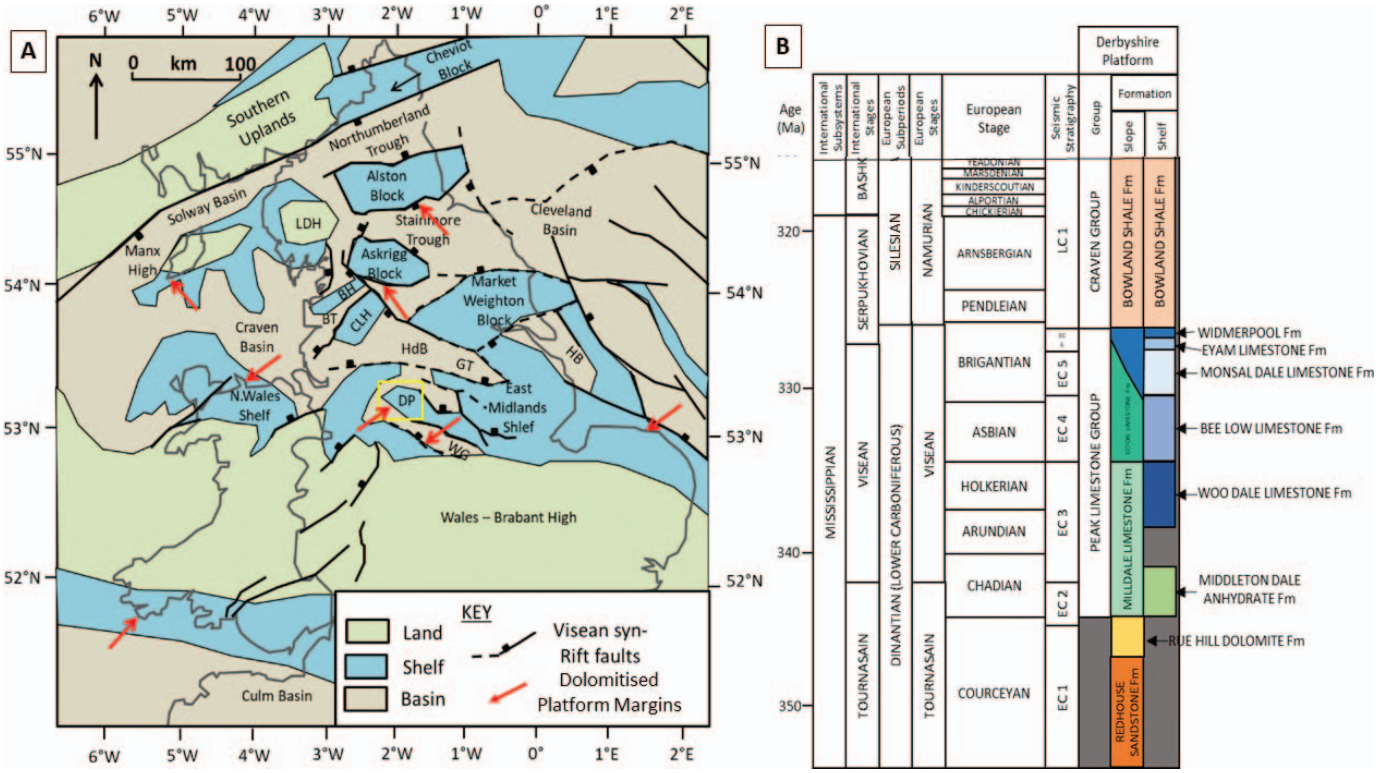

FIG. 1.—**A)** Tectono-stratigraphy of the Mississippian of southern Britain, after Fraser and Gawthorpe (2003). BH, Bowland High; BT, Bowland Trough; CLH, Central Lancashire High; DF, Dent Fault; DP, Derbyshire Platform; FHF, Flamborough Head Fault; GT, Gainsborough Trough; HdB, Huddersfield Basin; HB, Humber Basin; LDH, Lake District High; MCF, Morley–Campsall Fault; MH, Manx High; NCF, North Craven Fault; PF, Pennine Fault; SF, Stublick Fault; WG, Widmerpool Gulf. Approximate locations of dolostone bodies on the margins of carbonate platforms are indicated by the red arrows, with the yellow box highlighting the position of the Derbyshire Platform, the focus of this study. **B)** Stratigraphic framework for the Mississippian of the Derbyshire Platform. Ages derived from Gradstein and Ogg (2004), seismic sequences from Fraser et al. (1990).

occurred by downward-seeping brines in the Permo-Triassic whereas Schofield and Adams (1986), Ford (2002), and Hollis and Walkden (2012) proposed dolomitization from basinal brines expelled from juxtaposed hanging-wall basins.

Based on models of fluid flow and reactive transport models (RTM), Frazer (2014) and Frazer et al. (2014) recognized that while sufficient fluid volumes for dolomitization could have been supplied from basinal sediments in the hanging wall, such fluids probably contained insufficient magnesium to explain the observed volume of dolostone. Frazer (2014) showed that dolomitization could have occurred by geothermal convection of seawater along faults during platform growth, but to date there has been no petrographical or geochemical evidence to evaluate this hypothesis. As such, the current paper focuses on the first phase of dolomitization on the Derbyshire Platform and aims to a) determine the timing of the first phase of dolomitization, b) establish the source of fluid for dolomitization and c) evaluate the relationship between volcanism and dolomitization on the Derbyshire Platform.

GEOLOGICAL SETTING

Stratigraphy

During the Viséan, back-arc extension took place across the Pennine Basin, which was located north of the developing Variscan Orogen, with topography controlled by NE–SW, SW–NE trending faults (Fraser and Gawthorpe 2003). During this period, carbonate platforms developed on the footwalls of these reactivated Caledonian basement faults (Fraser and Gawthorpe 2003). The juxtaposed hanging-wall basins were filled progressively by pelagic and transported sediment during the Viséan–Serpukhovian. Post-rift thermal subsidence led to burial of the carbonate platforms to depths of 1–2 km beneath Bashkirian–Moscovian fluvio-deltaic systems that developed across a wide peneplain (Guion and Fielding 1988; Kelling and Collinson 1992). The entire basin was inverted in the Late Carboniferous to Permian, with the onset of the Variscan Orogeny (Fraser and Gawthorpe 2003).

The focus of this study is the southern margin of the Derbyshire Platform, which is composed of Viséan platform carbonates and syn-depositional, extrusive volcanics (Figs. 1A, 2A). The oldest exposed platform carbonates comprise the Holkerian Woo Dale Limestone Formation, a 105-m-thick succession of massive, fined grained, porcelaneous limestones (Fig. 1B). Overlying the Woo Dale Limestone Formation, the Asbian Bee Low Limestone Formation is composed of 75 m of skeletal packstone and grainstone. The Brigantian Monsal Dale Limestone Formation is at least 75 m thick, and is composed of gray to dark gray skeletal wackestone and packstone often containing chert (Aitkenhead and Chisholm 1982; Chisholm et al. 1983) (Fig. 1B). The limestone beds are separated by several volcanic tuff layers, one of which reaches 0.8 m in thickness at Masson Hill area (Ford 2001; Fig. 2B). The youngest carbonate sediments on the platform are limestones of the Eyam Limestone Formation, also of Brigantian age and ranging from 20 to 100 m in thickness. They are formed of thin, shelly limestones with shale partings with localized mud mounds (Ford 2002). The Viséan succession is overlain by the Serpukhovian-aged Millstone Grit Series, the total thickness of which is approximately 500 m. The total Upper Carboniferous cover is at least 1500 m and may have exceeded 2000 m (Smith et al. 1967; Aitkenhead et al. 1985).

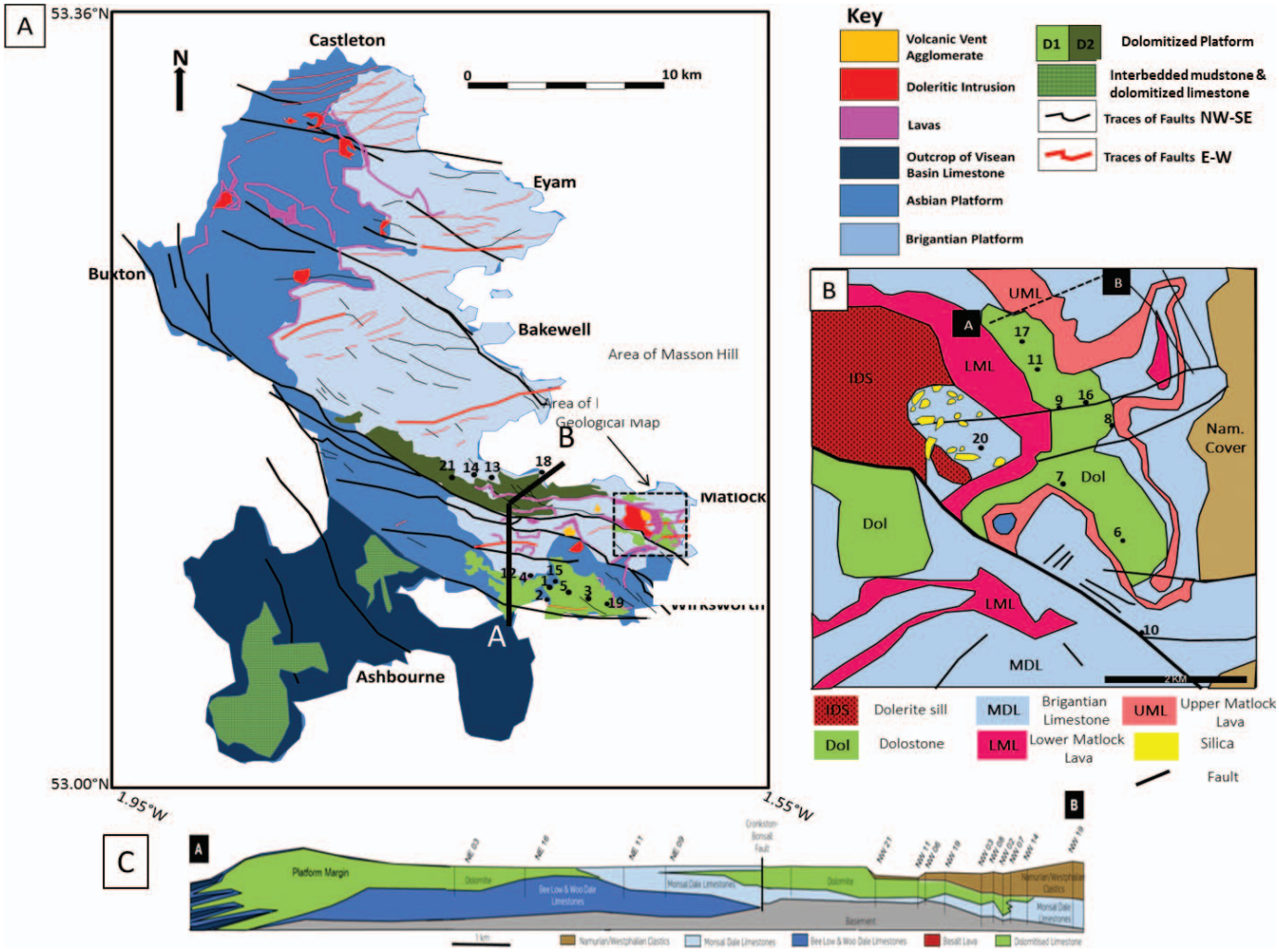

FIG. 2.—**A)** Geological map of the Derbyshire Platform. **B)** Detailed geological map of the Masson Hill area Sample localities and boreholes are identified on the maps. 1, Harborough Rocks; 2, Carsington Pastures; 3, Hopton Tunnel; 4, Brassington Moor Quarry; 5, Ryder Point Quarry; 6, Wapping Mine; 7, Upper Wood; 8, Temple Mine; 9, Coal Pit Rake; 10, Cromford; 11, Masson Hill; 12, High Peak Quarry; 13, Wyns Tor; 14, Grey Tor; 15, Golconda Mine; 16, Devonshire Cavern; 17, Masson Cavern; 18, Gurdall Wensley borehole; 19, Four Lanes End borehole; 20, Bottom Lees Farm borehole; 21, Gratton Dale. **C)** Cross section of line A–B, as shown in Part A.

Volcanism

Igneous activity during the Carboniferous was widespread across the UK from the early Viséan to the late Moscovian associated with lithospheric stretching (McKenzie 1978; Macdonald et al. 1984). On the Derbyshire Platform, extrusive volcanism was active in the Viséan (345–325 Ma) followed by intrusion of sills in the Serpukhovian (325–310Ma) (Macdonald et al. 1984). On the Derbyshire Platform, extrusive volcanism was concentrated around two main eruptive centers, Masson Hill and Miller's Dale (Macdonald et al. 1984). The southern volcanic center, concentrated at Masson Hill, has two major associated lavas; the Lower Matlock Lava (331–329 Ma), which forms the stratigraphic boundary between the Asbian and Brigantian, and the Upper Matlock Lava (330.9–329 Ma) (Macdonald et al. 1984; Fig. 2B). Away from the volcanic center, volcanic ash is present along karstic surfaces (Walkden 1972). The Lower Matlock Lava is a composite of several lava flows and tuffs, overlying the Bee Low Limestones (Chisholm et al. 1983) and is often taken as the boundary between the Asbian and Brigantian (Figs. 1B, 2B). The combined flows are about 45 m thick, but they reach 90 m thick at Masson Hill (Dunham 1952; Ixer 1975). Here, the lava appears to be in contact with the Bonsall dolerite intrusion with the thickness of the lava decreasing to the north and south from Masson Hill (Ford 2001). The Upper Matlock Lava lies in the center of the Monsal Dale Limestones, reaching 36 m in thickness (Smith et al. 1967; Ixer 1978) and averages 10–15 m elsewhere (Hurt 1968).

The geochemistry of the lavas indicates that volcanism was intra-plate and of tholeiitic affinity and they are composed of highly altered, fine-grained, vesicular, olivine-phyric and aphyric basalt (Walters and Ineson 1980; Macdonald et al. 1984). Both the lavas and the sills are enriched in light rare earth elements (LREE) in comparison to the heavy rare earth elements (HREE), with chondrite-normalized Ce (Ce_N) = 19–70 and Yb_N = 6–8. (Macdonald et al. 1984). Alteration of the primary igneous mineralogy probably resulted in the mobilization of Si, Ca, Mg, Na, K, Ba, Rb, and Sr, whilst Zr, Nb, Y, Ti , and P are interpreted to have been stable during alteration (e.g., Pearce and Cann 1973; Floyd and Winchester 1975; Pearce and Norry 1979; Macdonald et al. 1984).

Intrusive sills in the Masson Hill area, the Ible and Bonsall sills, are dated as Serpukhovian (325–310 Ma) and are medium to coarse-grained olivine dolerites (Macdonald et al. 1984). They commonly have serpentinized olivine phenocrysts, ophitic intergrowths of clinopyroxene (augite)

and plagioclase (labradorite), and an absence or rarity of vesicles and amygdales (Smith et al. 1967; Macdonald et al. 1984). Accessory minerals include Fe-Ti oxide and apatite in a microcrystalline matrix, with plagioclase and secondary chlorite and accessory nepheline recorded from the Bonsall Sill (Smith et al. 1967).

Diagenetic Framework of the Derbyshire Platform

The Viséan succession of the Derbyshire Platform displays a complex but well-constrained diagenetic history (Gutteridge 1987, 1991; Walkden and Williams 1991; Hollis 1998; Hollis and Walkden 2002). Four principal phases, or zones, of calcite cementation (Zones 1–4, as defined by Walkden and Williams 1991) were described from carbonate matrix porosity (Zones 1–4) and fractures (Zone 3–4) (Walkden and Williams 1991; Hollis and Walkden 2002). Zones 1–2 precipitated from meteoric water in the freshwater lens during platform growth, followed by Zone 3, which is interpreted to have precipitated in the shallow-burial realm from groundwater that was driven down depositional dip by topographic flow from the East Midlands Platform during the Serpukhovian (Walkden and Williams 1991). Zone 3 is volumetrically the most important cement phase, occluding macroporosity, and is succeeded by Zone 4 calcite which is interpreted to have co-precipitated with hydrocarbon, fluorite, sulfates and sulfide mineralization (Hollis and Walkden 1996 2002; Hollis 1998).

Dolomite on the Derbyshire Platform occurs in the Holkerian Woo Dale Limestone near the northern to central part of the platform (Schofield and Adams 1986), and as two distinct geobodies in the Asbian Bee Low Limestone and Brigantian Monsal Dale Limestone on the southern Derbyshire Platform (Fig. 2A, C). One of these bodies is near to the southern platform margin, while the other is elongate, following the NW–SE Cronston–Bonsall fault in the west, and associated with the Masson Hill volcanic center in the east (Fig. 2). A zone of dolomite has also been identified within the basinal succession to the southwest of the Derbyshire Platform (Fig. 2A), as described by Breislin (2018).

The Carboniferous limestone of the Derbyshire Platform hosts economic quantities of galena, fluorite, and barite mineralization, classified as Mississippi-Valley-Type (MVT) ore deposits (Ixer and Vaughan 1993; Ford and Quirk 1995). Minerals are hosted in matrix porosity, faults, and fractures in dolostones and limestones. The presence of ore bodies in igneous rocks and localized beneath lavas (Walters and Ineson 1980) suggests that the igneous bodies acted as aquitards, as well as hosts to the mineralization (Walters and Ineson 1980; Ford 2002). Mineralization in the Lower Carboniferous of the Derbyshire Platform commonly occurs at dolostone–limestone boundaries, suggesting a spatial association of dolostone reaction fronts and mineralization (Ford 2002). A conceptual model of fluid flow as a result of overpressure release and seismic valving of fluids from the hanging-wall basins onto the Derbyshire Platform has been proposed based on the distribution of fracture-controlled calcite cementation and associated hydrocarbon, galena, fluorite, and barite mineralization (Coleman et al. 1989; Ixer and Vaughan 1993; Hollis and Walkden 2002).

METHODS

Rock samples were collected from fifteen outcrops, five mines, and three boreholes (Fig. 2A) in the Asbian to Brigantian succession of the Matlock area. The area was geologically mapped and logged, with detailed petrographic analysis of thin sections prepared from samples. Each locality and core was sampled systematically to cover the stratigraphic range and diversity of lithofacies and logged to record texture and composition, sedimentary features, skeletal content, and diagenetic features. A total of 53 polished thin sections were prepared from resin-impregnated subsamples (Table 1).

All thin sections were examined using optical transmitted-light and cathodoluminescence (CL) microscopy and scanned using an EPSON Perfection V600 Photo at 2400 dpi resolution. Optical microscopy was undertaken using a Nikon Eclipse LV100NPOL microscope fitted with a Nikon DS-Fi2 camera. Dolomite textures were described according the scheme of Sibley and Gregg (1987). CL observations were made using a CITL CCL 8200 Mk3 cold optical cathodoluminescence system coupled with a Progress C10 Laser Optik digital photographic system. Operating conditions for CL were set to 10 kV and 300 μA at a pressure of c. 0.2 Torr and maintained by microcomputer control.

Fluid-inclusion screening was conducted on selected dolomite samples using a Nikon Eclipse LV100NPOL microscope to determine the phases present in primary and pseudo-secondary inclusions, and their distribution in crystals. Based on the observation that the primary inclusions contain single-phase fluid inclusions, fluid-inclusion microthermometry was not conducted.

Standard X-ray diffractometry (XRD) was conducted on powders, acquired using a precision drill. These were then prepared following the methods of Charlier et al. (2006). The analysis was carried out using a Bruker D8Advance diffractometer at the University of Manchester. A tube voltage of 40 kV and a tube current of 40 mA, with a step size of 0.02° and time constant of 2.00 seconds was employed, using CuKα radiation. Semi-quantitative estimates of bulk mineralogy fractions were carried out using peak-area measurements (*sensu* Schultz 1964). All results contain an analytical error of 0.5%. Dolomite stoichiometry (%mol $MgCO_3$) was calculated using the methodology of Jones et al. (2001) to determine the amount of calcium in excess of stoichiometric ($Ca_{50}Mg_{50}$) based on the position of the dolomite 104 reflection.

Inductively coupled plasma mass spectrometry (ICP-MS) analysis was conducted on powdered samples of host-rock limestone, bulk dolostone, and individual cement zones. Powders were digested in 2 ml of 20% HCl before dilution to 2% HCl. In addition, two blank samples were prepared in the same way to ensure reproducibility. Corresponding samples were drilled from hand specimens and their mineralogy checked using XRD to ensure no contamination in dolostone samples by calcite cements. REEs and Y concentrations were measured using ICP-MS with an Agilent 7500cx mass spectrometer. Samples were run against internal standards and reproducibility of 0.1‰ (1σ). All samples are reported in mg/l or ug/l (ppm or ppb). All REE results have been PAAS normalized following the methods of Nance and Taylor (1976).

Stable oxygen and carbon isotope analysis was conducted on powdered samples of dolostone, limestone, brachiopods, and discrete cement phases, acquired using a tungsten-tipped dentist drill. The mineral composition of the samples was assured by XRD analysis of a small amount of powder to ensure that there was no analysis of mixed calcite–dolomite samples. Samples of calcite were reacted (to completion) with phosphoric acid under vacuum, at temperatures of 25° C (*sensu* McCrea 1950). Gases were measured by dual-inlet, stable-isotope-ratio mass spectrometry using a VG SIRA10 mass spectrometer. Isotope ratios were corrected for ^{17}O effects following the procedures of Craig (1957). In order to calculate precipitation temperatures and fluid $\delta^{18}O$ compositions, the equilibrium oxygen isotope fractionation of Friedman and O'Neil (1977) was used for calcite samples and the equilibrium fractionation factor of Matthews and Katz (1977) was used for dolomite samples. Samples were run against an internal standard, and all results were reproducible to ± 0.1‰ (2σ). All isotope data are reported relative to the VPDB calcite standard.

Strontium isotope analysis was conducted on powdered whole rock dolostone and discrete dolomite cements obtained using a tungsten-tipped micro-mill following the methodology of Charlier et al. (2006) and Pollington and Baxter (2010). Sample mineralogy was checked by XRD. Sr (Oak Ridge ^{84}Sr, 1.1593 ppm) and Rb spikes were added to each sample to boost the signal. Strontium was extracted from the rock powders for isotopic analysis using Sr Spec extraction chromatographic resin. Column

TABLE 1.—*Summary data of calcite cement zones (data form Walkden and Williams 1991; Hollis and Walkden 2002), and dolostone phases D1, D2, D3, D4, and D5 observed on the Derbyshire Platform.*

Sample Name	Well/Location	Lithology	Thin Section	XRD	ICP MS	C&O Isotopes	Sr Isotopes
SSK56632	Carsington Pastures Wind Farm RC-T1-08	Dolomite	x	x		x	x
SSK56633	Carsington Pastures Wind Farm RC-T1-08	Dolomite	x				
SSK56634	Carsington Pastures Wind Farm RC-T1-08	Dolomite	x				
SSK56639	Carsington Pastures Wind Farm RC-T1-08	Dolomite	x				
SSK56642	Carsington Pastures Wind Farm RC-T1-10	Dolomite	x				
SSK56643	Carsington Pastures Wind Farm RC-T1-10	Dolomite	x				
SSK56644	Carsington Pastures Wind Farm RC-T1-10	Dolomite	x	x			x
SSK56648	Carsington Pastures Wind Farm RC-T4-07	Dolomite	x				
SSK56650	Carsington Pastures Wind Farm RC-T1-17	Dolomite	x				
SSK56652	Carsington Pastures Wind Farm RC-T1-17	Dolomite	x				
SSK56653	Carsington Pastures Wind Farm RC-T1-17	Dolomite	x				
SSK56656	Carsington Pastures Wind Farm RC-T1-11	Dolomite	x				
SSK56657	Carsington Pastures Wind Farm RC-T1-11	Dolomite	x				
SSK56659	Carsington Pastures Wind Farm RC-T1-11	Dolomite	x				
SSK56661	Carsington Pastures Wind Farm RC-T1-11	Dolomite	x				
SSK56662	Carsington Pastures Wind Farm RC-T1-11	Dolomite	x	x		x	x
SSK56675	Carsington Pastures Wind Farm RI-T3-1A	Dolomite	x				
SSK56679	Carsington Pastures Wind Farm RI-T3-1A	Dolomite	x				
SSK56693	Carsington Pastures Wind Farm RC-T2-13	Dolomite	x	x			x
GD_11_3_15_02	Gratton Dale	Limestone	x		x		
GD_11_3_15_03	Gratton Dale	Limestone	x				
GD_11_3_15_04	Gratton Dale	Dolomite	x		x	x	
PQ_12_3_15_01	Peak Quarry	Limestone	x				
HGC_12_3_15_01	Hoe Grange Cutting	Dolomite			x	x	
BQ_13_3_15_01	Brassington Quarry	Limestone	x		x	x	
BQ_13_3_15_02	Brassington Quarry	Dolomite	x	x		x	x
HR9	Harborough Rocks	Dolomite	x	x	x	x	x
HR6	Harborough Rocks	Dolomite	x		x		
HR7	Harborough Rocks	Dolomite	x		x		
HR_14_3_01	Harborough Rocks	Dolomite	x		x		
HR_14_3_05	Harborough Rocks	Dolomite	x	x		x	x
BMQ_16_3_15_04	Brassington Moor Quarry	Dolomite	x		x		
RPQ_20_3_15_01	Ryder Point Quarry	Dolomite	x	x	x	x	x
HR_20_3_15_02	Harborough Rocks	Dolomite			x	x	
BC_01	Brundcliffe Cutting	Limestone	x	x	x	x	x
NHC_01	Newhaven Cutting	Limestone	x		x	x	
WT_01	Wyns Torr	Dolomite	x	x	x	x	x
WT_02	Wyns Torr	Dolomite	x	x	x		x
MT_02	Middleton Top Quarry	Limestone			x		
MT_03	Middleton Top Quarry	Limestone		x	x		x
HR_14_3_02	Harborough Rocks	Dolomite	x			x	
HR20_3_02	Harborough Rocks	Dolomite	x				
HR1A	Harborough Rocks	Dolomite	x			x	
HR1F	Harborough Rocks	Dolomite	x				
HR1B	Harborough Rocks	Dolomite		x			x
HR_25_06_04	Harborough Rocks	Dolomite	x				
HGC_01	Hoe Grange Cutting	Dolomite	x	x		x	x
HGC_02	Hoe Grange Cutting	Limestone	x	x		x	x
HGC_03	Hoe Grange Cutting	Limestone	x				
HGC_04	Hoe Grange Cutting	Limestone	x				
HGC_05	Hoe Grange Cutting	Limestone	x				
WM22	Wapping Mine	Dolomite	x		x	x	x
WM21	Wapping Mine	Dolomite	x			x	x
CPR2	Coal pit Rake	Limestone				x	x
TM8	Temple Mine	Dolomite	x		x	x	x
CPR3	Coal pit Rake	Dolomite	x		x	x	x
TM5	Temple Mine	Dolomite	x			x	x
TQ1	Temple Quarry	Dolomite			x	x	x
UW1	Upper Wood	Dolomite	x		x	x	x
GW1	Gurdall Wensley	Dolomite	x		x	x	x
GW3	Gurdall Wensley	Dolomite	x		x	x	
GW4A	Gurdall Wensley	Dolomite				x	x
GW4B	Gurdall Wensley	Dolomite				x	
BH13	Ballidon Hill	Dolomite				x	
SLK72	Standlow Lane Kniveton	Dolomite				x	
FL41	Four Lanes Wirksworth	Dolomite				x	
FL42	Four Lanes Wirksworth	Dolomite				x	
		Total	**53**	**14**	**24**	**32**	**24**

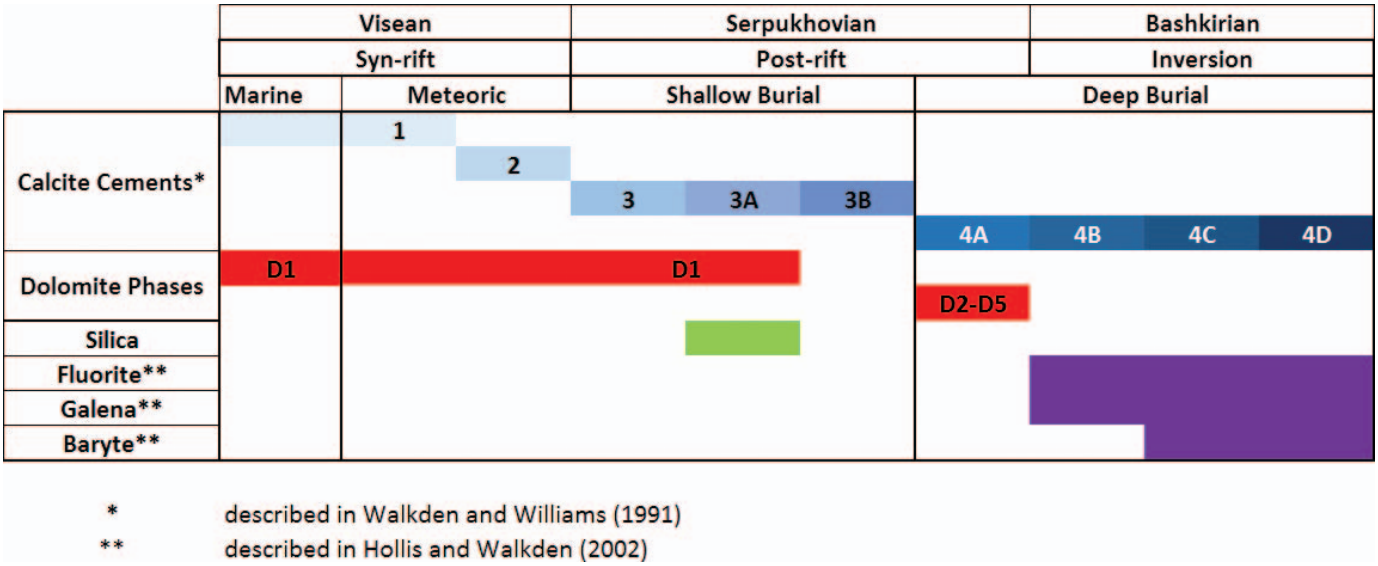

FIG. 3.—Paragenetic sequence for the Derbyshire Platform. Note that calcite cements (Z1–4) were defined by Walkden and Williams (1991), and the paragenesis and intergrowth of Zone 3A–B and 4A–D calcite cements with non-carbonate minerals was defined and described by Hollis and Walkden (2002).

preparation and chemical separation were conducted following the methods of Deniel and Pin (2001) and Charlier et al. (2006). Before analysis, the Sr samples were mixed with tantalum (Ta) emitter solution, loaded on to single Rhenium (Re) filaments and subjected to a 2A current. Sr isotope ratios were measured on the British Geological Survey (NIGL) Thermo-Finnigan Triton TIMS instrument in static collection mode. An internal NBS 987 standard was used for calibration with a reproducibility of + 0.1%0 (2σ). During TIMS analysis, spiked samples are run in the same fashion as unspiked samples. However, the results of spiked samples were corrected, off-line, for spike contribution. All results are reported to the NBS 987 standard.

RESULTS

Distribution of Dolostone

Both fabric-selective, stratabound dolostone and fabric-destructive, non-stratabound dolostone were observed on the Derbyshire Platform. Five unique dolomite textures are identified (D1–D5; Table 1, Fig. 3). Phases D1–D3 are replacive phases; D1, the principal focus of the current study, is the oldest phase and is cross-cut and replaced by D2, which is itself cross-cut by D3. Phases D4 and D5 are dolomite cements that are identified petrographically. Based on the mapped distribution of D1 from outcrop and core, it is estimated to form 50% of the total volume of dolostone on the Derbyshire Platform (Fig. 2C). The thickest section of D1 is observed at the platform margin in Golconda Mine, where it is approximately 120 m thick. Away from the platform margin, on the platform top, the thickness of D1 decreases to an average of around 40 m (Fig. 2C).

D1 dolostone occurs in platform-margin grainstones and packstones and commonly occurs along or near to, the southern margin of the Derbyshire Platform (Fig. 2A). In outcrop, D1 is buff-gray, with a sucrosic texture. It is fabric preserving, with retention of bedding, cross-lamination, and bioturbation (Fig. 4). D1 dolostone is best exposed at Harborough Rocks, where an upward-shallowing succession of facies has been pervasively dolomitized; a basal layer of slumped and dewatered beds is overlain by pervasively bioturbated beds (by *Thalassinoides*) and capped by crinoidal and coral-bearing grainstones. Vuggy and moldic porosity is abundant, and D1 dolostone is cross-cut by stylolites. Elsewhere, the dolostone is occasionally overprinted by D2 and D3 (Figs. 4A, 5A). Reaction fronts are diffuse (Fig. 4A), with patchy dolomite bodies ranging from 5–30 cm in diameter, occurring up to 3 m away from the main dolostone body.

D1 dolostone also occurs in isolated reef mounds in the platform interior at Wyns Tor and Grey Tor and adjacent to extrusive Viséan lavas in the Matlock Volcanic Complex (Fig. 2B). In the Matlock area, D1 is strongly stratabound, preferentially forming both above and below the Upper and Lower Matlock Lavas, and above tuffs (Fig. 4C, D), as well as above or below exposure surfaces. Galena–fluorite–barite–calcite mineral assemblages are observed at the contact between dolostone and limestone, as well as along exposure surfaces. In Wapping Mine, at the center of the Matlock Volcanic Complex, dolostone replaces limestone, and white, opaque dolomite cement also occurs within a fault breccia along an E–W oriented fault (Fig. 5B, C). At Cromford (Fig. 5A), within the Masson Hill area, several E–W oriented faults formed as splays to the NW–SE Cronkston–Bonsall fault, with horizontal slickensides providing evidence of lateral movement. These E–W faults host D1 dolostone, including dolomite-cemented breccias. Dolomite cement is cross-cut by calcite, fluorite, barite, and minor galena, with slickensides that indicate strike-slip movement.

The structural lineaments on the Derbyshire Platform are predominantly NW–SE and NE–SW oriented crustal faults, with associated E–W and N–S trending faults (Figs. 2, 3). The Cronkston–Bonsall fault is a major NW–SE trending, deep-seated crustal fault, which extends approximately 20 km from the NW of the Derbyshire Platform (near the town of Buxton), to the Masson Hill area in the SE (Fig. 2). It is slightly sinuous and locally compound in nature, with several parallel faults and associated splays. Replacement of the host rock by fabric-destructive, non-stratabound (D2) dolostone with non-planar textures occurs along the length of the Cronkston–Bonsall Fault.

N–S faults cross-cut the E–W oriented faults, and are surrounded by a halo of non-fabric selective, non-planar dolostones up to 50 cm wide, and classified as D3 dolostone (Fig. 5A). At the intersection of E–W and N–S faults, large cavities up to a meter in diameter are filled with calcite, fluorite, and barite. Brecciation is commonly observed along these N–S faults, with the matrix commonly hosting galena and fluorite (Fig. 5C). The N–S faults also display slickensides, indicating strike-slip movement, and have greater quantities of sulfide and fluorite mineralization than the E–W oriented faults.

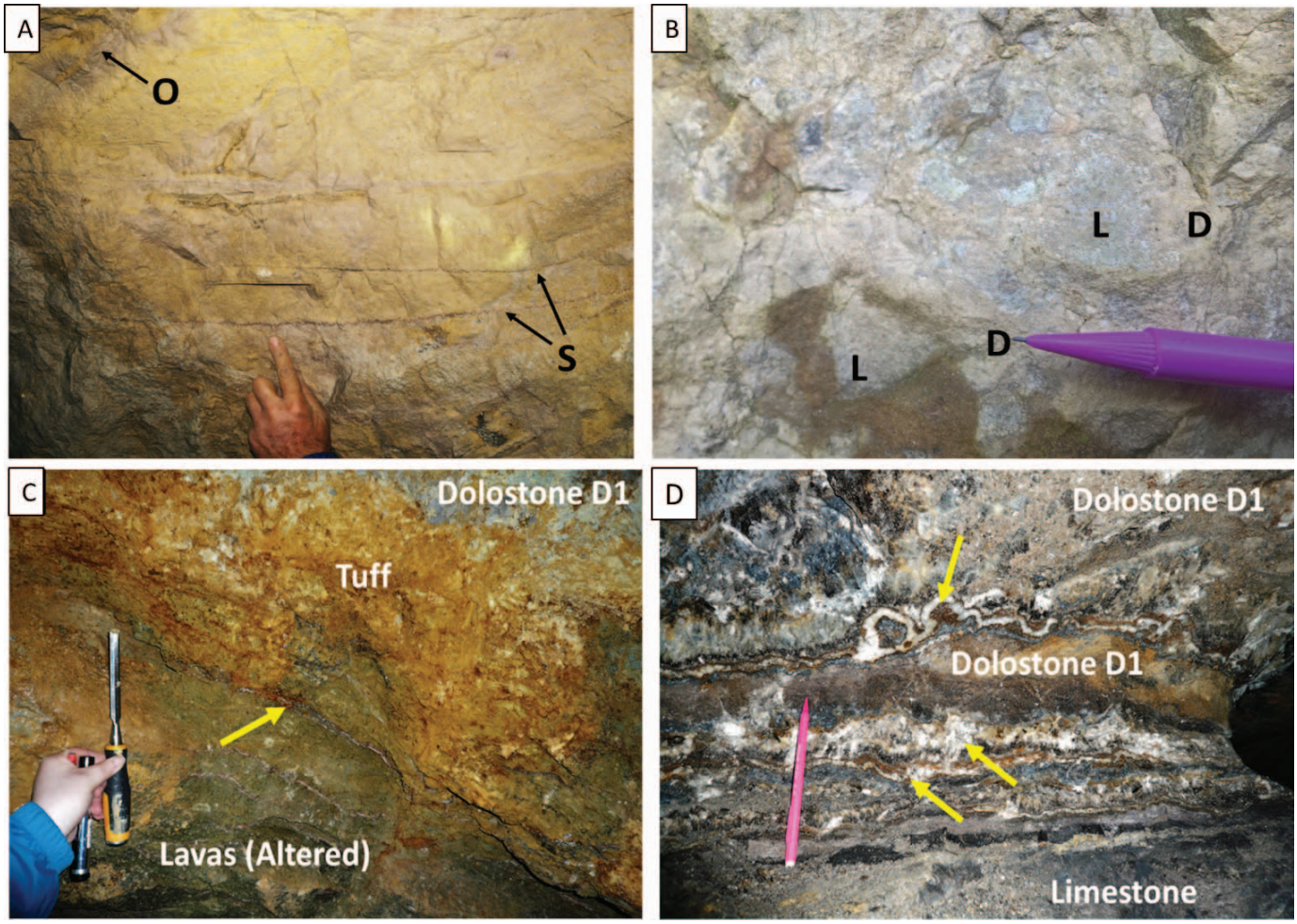

FIG. 4.—Dolostone texture. **A)** Sucrosic, buff-gray dolostone within platform margin facies. Horizontal stylolites are seen to cross-cut dolostone (S). Around cross-cutting fractures, there is a texture change to gray fine-crystalline dolostone. This is overprinted by later dolostone phases (O). **B)** Partial dolomitization (D) of limestone (L). **C)** Relationship between D1 dolostone and with dolostone D1 occurring above the Lower Matlock Lava (lavas, altered) and associated tuff. Lavas are heavily altered, showing a green color. Contact between the lava and the tuff is sharp (arrowed) whilst the boundary between the tuff and dolostone is diffuse. Dolostone D1 is buff-gray above the lavas. **D)** Calcite, barite, and galena mineralization (arrowed) at dolostone–limestone boundary in Masson Cavern (Location 11 in Fig 2).

Petrographic and Crystallographic Characteristics of D1 Dolostone

In thin section, D1 dolostone is fabric destructive, with dolomite crystal size preserving a subtle fabric in packstone facies; in grainstone facies, dolomitization is fabric destructive in thin section. D1 is composed of clean, limpid, planar-e to planar-s dolomite (*sensu* Sibley and Gregg 1987). The coarsest dolomite crystals (up to 1.45 mm diameter) are in allochem-rich grainstones towards the platform margin, whereas crystal size is smallest (approx. 0.1 mm) where replacement of micrite matrix occurred. Crystals become more euhedral as crystal size increases. Fluid inclusions in these crystals are single phase. Where dolomitization is incomplete, individual dolomite crystals occur in micritized allochems; where dolomitization is pervasive, dolomite crystals form a lining to the base of crinoid molds (Fig. 6B). The dolomite has a distinct yellow-orange cathodoluminescence, with small, red luminescent inclusions (Fig. 6B). Where recrystallization by D2 and D3 dolomite has occurred, non-planar textures are more common, alongside a change from orange to red luminescence in CL. Dull luminescent, sparry, pore-filling calcite cement (Zone 3 calcite cement of Walkden and Williams 1991) is not observed in D1 dolostone, although it is present in minor volumes within adjacent limestones (Fig. 6C, D).

Volcanics

Lava samples were taken from Temple Mine, Gratton Dale, and Gurdall Wensley borehole (Fig. 7). The lavas from Temple Mine in the Masson Hill Volcanic Complex are highly altered, with less intense and very minor alteration observed in the samples from Gurdall Wensley and Gratton Dale, respectively. The lavas are commonly vesicular, fine-grained olivine basalts containing amygdales of carbonate or chlorite (Fig. 7A–D). Where unaltered, the primary igneous mineralogical assemblage is composed of olivine, clinopyroxene, orthopyroxene, and plagioclase. The lavas are highly brecciated and cut by calcite-cemented fractures.

Petrographical and XRD analyses shows that primary olivine and pyroxene has been altered to clay minerals, (illite, chlorite–smectite, and kaolinite), calcite, Fe-oxide, chlorite, quartz, and minor pyrite (Fig. 7C) with pyroxenes commonly replaced by chlorite or calcite (Fig. 7B). This alteration is evidenced in hand specimen by a change from dark gray-green to a paler and greener color (Fig. 7A). Calcite cement occludes amygdales, and has replaced the matrix of the lava as anhedral, poikilotopic crystals up to 2 mm in diameter. There are monomineralic chlorite reaction rims around these calcite-filled amygdales, with the calcite displaying

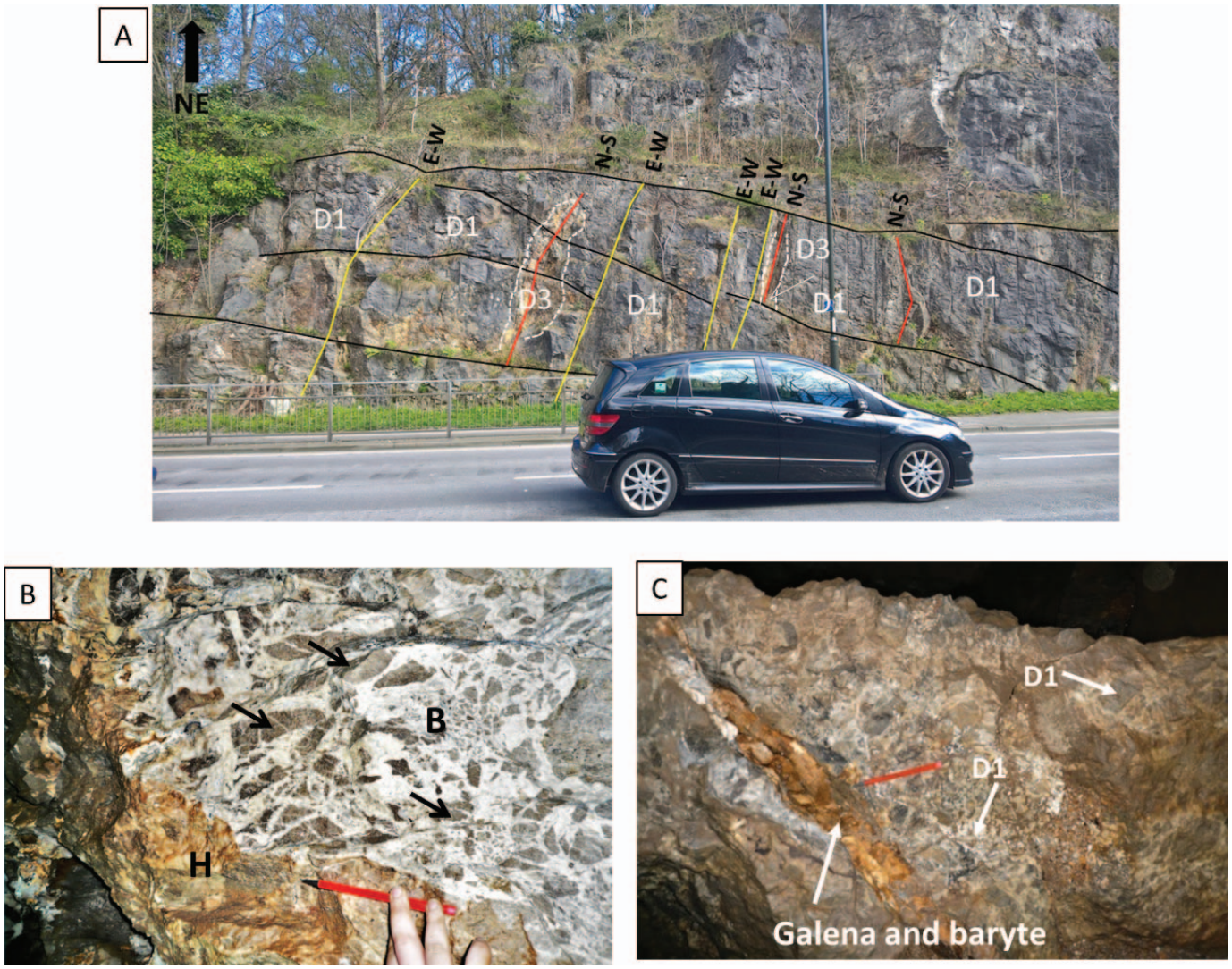

FIG. 5.—**A)** View looking northeast of east–west-trending cliff section up to 15 m high, car (Nissan Note) is 4.1 m long, approximately 3 m away from the cliff face, showing two sets of faults. Set 1: E–W oriented faults, highlighted in yellow, cemented, planar, gently dipping (0–10°), 5 m+ in length, 1–10 cm in width, and 1–6 m spacing. Set 2: N–S oriented faults, highlighted in red, cemented, planar, gently dipping (0–10°), 5 m+ in length, 1–30 cm in width, and 1–6 m spacing. **B)** Dolostone D1 in fault breccia in Wapping Mine (location 6 in Fig. 2). Host rock (H) is dolomitized, as are rotated wall fragments (arrowed) in the fault breccia (B) with a dolomite cement. **C)** Galena and barite mineralized fracture cross cutting dolostone breccia in N–S trending fault in Wapping Mine.

metasomatic textures (Fig. 7D). Under CL, the calcite has a yellow-orange color.

Silicification and Mineralization

Silicified limestone was observed on the Masson Hill anticline, on the southeast platform margin (Fig. 2), as well as parallel to an E–W oriented fault at Gratton Dale. These localities are proximal to the Viséan extrusive volcanic horizons at Gratton Dale and Masson Hill (Fig. 2). In the field, silicification is not facies selective, but occurs as discrete bodies, up to 5 m in diameter, located at the apex of the Masson Hill anticline, and close to faults. The silica is replacive, forming an anhedral mosaic composed of 0.5-mm-size crystals, where it is most pervasive. There is usually a diffuse boundary between silicified and unaltered limestone (Fig. 7E). Where silicification is incomplete, individual crystals are euhedral and finely crystalline (0.1–0.3 mm) (Fig. 7F). Although replacive silica and D1 dolostone are not observed together, intercrystalline porosity and fractures containing fluorite, barite, and calcite, cross-cutting silicified limestone and D1 in horizontal, sub-vertical and vertical fractures, are seen (e.g., Golconda Mine, Temple Mine, High Peak Quarry, Masson Cavern in Fig. 2), particularly at the boundary between dolostone and limestone. Therefore, both D1 dolomite and silica predate mineralization, but the paragenetic relationship between D1 dolostone and silica is equivocal.

Geochemistry

D1 dolostone is nearly stoichiometric with $MgCO_3$ = 47.9 to 51.2%, with an average of 50.5%. Isotopic data is summarized in Table 3. The isotopic signature of unaltered brachiopod shells ranges from $\delta^{13}C = 0.3$ to 0.8‰ VPDB and $\delta^{18}O = -4.1$ to –4.2‰ VPDB (n = 2) and whole-rock limestone from $\delta^{13}C$ = 1.4 to 0.8‰ VPDB and $\delta^{18}O$ = –5.2 to –3.2‰ VPDB (n = 5). Dolostone ranges from $\delta^{13}C = -2.7$ to 0.8‰ VPDB and $\delta^{18}O = -2.8$ to –5.01‰ VPDB (n = 23). The mean $\delta^{13}C$ values ($\delta^{13}C$ = –0.6‰ VPDB, n = 23) of the dolostone are more depleted than those of whole-rock limestone and brachiopods ($\delta^{13}C$ = 2.2‰ and 0.5‰ VPDB, respectively). There is a spatial variation in $\delta^{18}O_{dolostone}$, with more

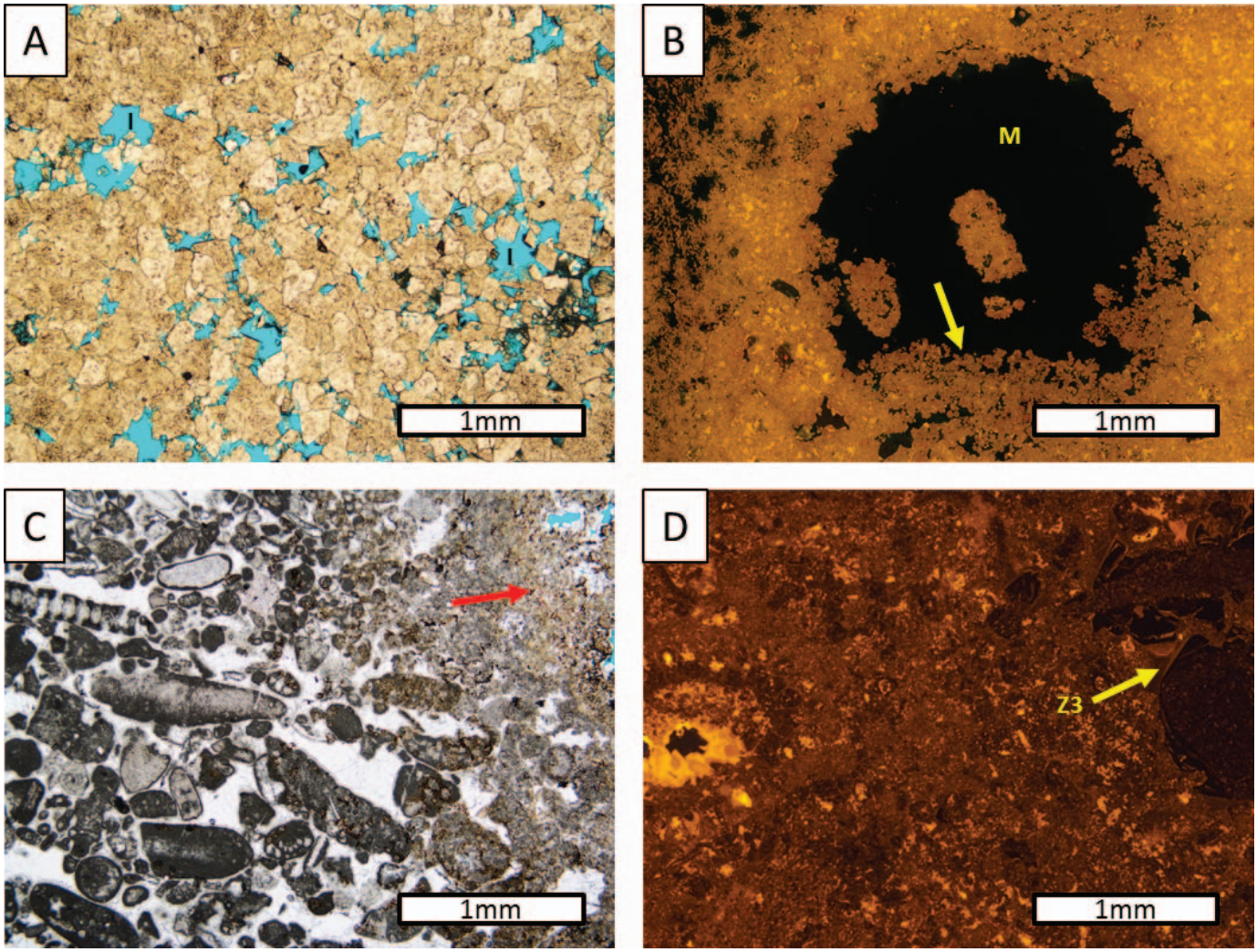

FIG. 6.—Dolostone petrography. **A)** Photomicrograph, PPL, dolomitized grainstone composed of clean, limpid, planar-e to planar-s dolostone rhombs, intercrystalline porosity (I). **B)** Photomicrograph, CL, showing distinctive yellow-orange luminescence of dolomite, with moldic porosity (M) and dolomite sediment at the bottom of a crinoid mold (arrowed). **C)** Photomicrograph, PPL, partially dolomitized skeletal pack–grainstone. Dolomite crystals are seen to form in micrite matrix (arrowed). Pore-filling cements are Zone 1–3 calcite cement. **D)** Photomicrograph, CL, un-dolomitized platform margin limestone. Only minor amounts of Zone 3 cement as described by Walkden and Williams are visible (Z3, arrowed).

depleted values ($\delta^{18}O$ = –4.1‰ VPDB, n = 11) in the Matlock area, proximal to the volcanic center and extrusive volcanics, compared to the platform margin ($\delta^{18}O$ = –3.4‰ VPDB, n = 12). No spatial trend is observed in the $\delta^{13}C$ of the dolostone. The dolomite cement taken from the E–W fault breccia has one of the lowest mean $\delta^{13}C$ and $\delta^{18}O$ values of all the investigated dolostones ($\delta^{13}C$ = –1.52‰ VPDB, $\delta^{18}O$ = –5.01‰ VPDB, respectively) and dolomitized wall rock adjacent to this fault also has a light isotopic signature ($\delta^{13}C$ = 0.28‰ VPDB, $\delta^{18}O$ = –4.79‰ VPDB). Calcite cement precipitated in amygdales in the lavas are more depleted than Viséan seawater ($\delta^{13}C$ = –1.6‰ VPDB and $\delta^{18}O$ = –3.0‰ VPDB).

TABLE 2.—*Summary of the five dolostone phases identified on the Derbyshire platforms and their structural relationships.*

Phase	Distribution	Occurrence	Structural trend	Volume
D1	Stratabound	Replacive	E–W	50%
D2	Non-stratabound	Replacive	NW–SE	40%
D3	Non-stratabound	Replacive	N–S	< 10%
D4	Non-stratabound	Cement	NW–SE, N–S, NE–SW	< 5%
D5	Non-stratabound	Cement	NW–SE, N–S, NE–SW	< 5%

Unaltered brachiopod shells have $^{87}Sr/^{86}Sr$_tr 0.7078 (± 0.00004) that matches Viséan seawater (Burke et al. 1982). Average dolostone $^{87}Sr/^{86}Sr$ = 0.7084 (± 0.00004, n = 13) are more radiogenic than seawater, with a slight spatial trend whereby more radiogenic dolostone is recorded at the Matlock Volcanic Complex ($^{87}Sr/^{86}Sr$ = 0.7083 (± 0.00004, n = 3) (Fig. 8) compared to the platform margin at Harborough Rocks and platform-interior isolated reefs ($^{87}Sr/^{86}Sr$ = 0.7085 (± 0.00004, n = 10). The strontium signature of unaltered basalt taken from Gratton Dale is significantly less radiogenic than seawater at $^{87}Sr/^{86}Sr$ = 0.7046 (± 0.00004, n = 1; Fig. 8A). Altered lavas sampled from the Matlock Volcanic Complex have a strontium signature close to Viséan seawater at $^{87}Sr/^{86}Sr$ = 0.7080 (± 0.00004, n = 1).

Total REE concentrations (ΣREE + Y) in the dolostone range from 1.41 to 11.35 ppm, and are lower than that observed within the whole rock limestone samples, (4.93 to 77.5 ppm) (Fig. 9B, C). REE patterns are similar for all dolostone samples analyzed, both at the platform margin and

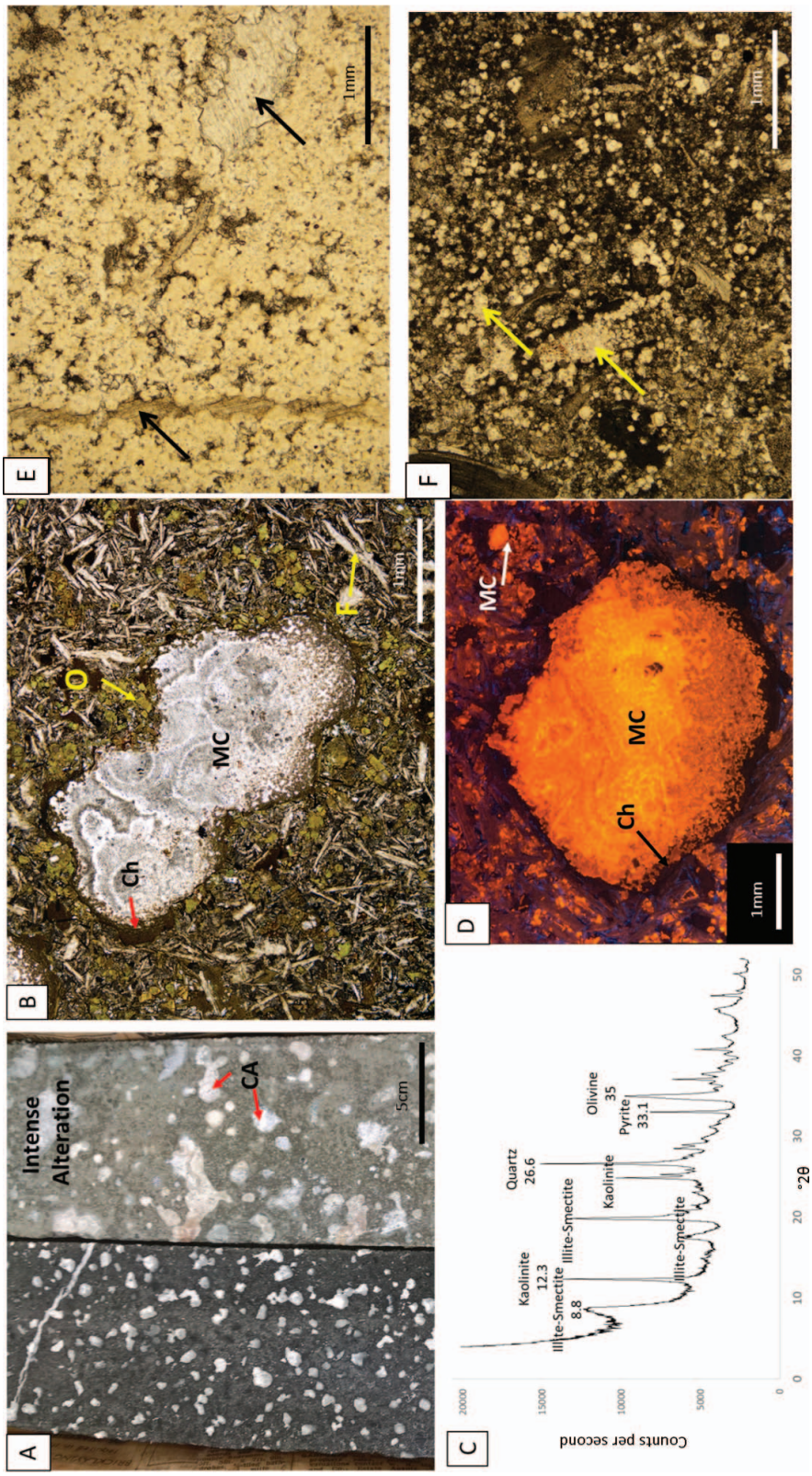

FIG. 7.—Viséan extrusive lavas in the Masson Hill area. **A)** Core photo of lava showing calcite amygdales in the basalt (CA). Core on the right-hand side of the image is more intensely altered that the core on the left-hand side. **B)** Thin-section micrograph, PPL, amygdale in altered basalt matrix. The amygdale is lined by chlorite (Ch) and filled with calcite displaying a metasomatic texture (MC). Basalt matrix contains feldspars (F) and altered olivine (O). **C)** XRD traces of the altered lavas showing presence of illite–smectite, kaolinite, quartz, and pyrite, as well as olivine. **D)** Thin section micrograph, CL, chlorite rim to amygdale is non-luminescent, with metasomatic calcite displaying bright CL. Metasomatic calcite is also seen within the matrix replacing primary minerals (MC). **E**, **F)** Thin-section micrograph showing almost complete replacement of limestone by quartz. Remaining calcitic allochems are arrowed.

TABLE 3.—*Carbon and oxygen isotope compositions of the investigated limestone, brachiopods, calcite, and dolostone samples.*

Location	Sample Number	Mineralogy	$10^3\ \delta^{13}C_{VPDB}$	$10^3\ \delta^{18}O_{VPDB}$
Ballidon Hill	BH13	limestone	1.6	–3.2
Brassington Quarry	BQ-01	limestone	1.4	–5.6
Carsington Pastures	SSK 56662	D1 dolostone	–1.4	–3.1
Carsington Pastures	SSK 56632	D1 dolostone	–2.5	–3.1
Coal Pit Rake	CPR2	D1 dolostone	–1.3	–3.9
Coal Pit Rake	CPR3	D1 dolostone	–0.7	–4.1
Four Lanes Wirksworth	FL42	brachiopod	0.3	–4.1
Four Lanes Wirksworth	FL41	brachiopod	0.8	–4.2
Gratton Dale	GD-11-3-04	limestone	3.5	–5.3
Gurdall Wensley	GW7	calcite amygdale	–1.6	–3.0
Gurdall Wensley	GW4B	D1 dolostone	–0.3	–3.6
Gurdall Wensley	GW4A	D1 dolostone	–0.3	–3.7
Gurdall Wensley	GW1	D1 dolostone	–1.9	–3.8
Gurdall Wensley	GW3	D1 dolostone	–0.7	–4.1
Harborough Rocks	HR14-3-05	D1 dolostone	–0.7	–2.8
Harborough Rocks	HR9	D1 dolostone	–0.8	–3.0
Harborough Rocks	HR6	D1 dolostone	–1.4	–3.1
Harborough Rocks	HR7	D1 dolostone	–0.8	–3.2
Harborough Rocks	HR14-3-01	D1 dolostone	–1.5	–3.3
Harborough Rocks	HR20-3-02	D1 dolostone	–1.5	–3.5
Harborough Rocks	HR1A	D1 dolostone	0.4	–3.7
Harborough Rocks	HR1F	D1 dolostone	0.8	–3.9
Harborough Rocks	HR1B	D1 dolostone	–0.2	–4.0
Longcliffe	LC62	limestone	1.4	–5.5
Ryder Point Quarry	RPQ-20-3-01	D1 dolostone	–0.7	–3.6
Standlow Lane Kinveton	SLK72	limestone	3.2	–4.2
Temple Mine	TM8	D1 dolostone	1.0	–4.1
Temple Mine	TM5	D1 dolostone	1.1	–4.3
Temple Quarry	TQ1	D1 dolostone	0.1	–4.3
Upper Wood	UW1	D1 dolostone	–1.4	–4.6
Wapping Mine	WM21	D1 dolostone	0.3	–4.8
Wapping Mine	WM22	D1 cement	–1.5	–5.0

from samples in the Matlock Volcanic Complex (Fig. 9). Most dolostone and limestone samples display a negative Ce anomaly, and a slight middle rare earth element (MREE) bulge (Fig. 9C). Y/Ho ratios for whole-rock limestone range from 30.4 to 38.5, and are slightly higher in dolostone (D1 platform margin = 37.3–49.4; D1 Matlock Volcanic Complex = 35.8–51.2).

Interpretation

Paragenesis

Several features are consistent with dolomitization in a near-surface or shallow-burial setting. Firstly, D1 is dominated by planar-e and -s dolomite crystals that contain mono-phase primary fluid inclusions. Secondly, D1 is fabric retentive and stratabound and occurs only in platform-margin grainstones and packstones, or along syn-depositional E–W oriented faults, suggesting a depositional and structural control on dolomitization. The presence of dolostone both above and below lavas in the Masson Hill area strongly suggests that lavas controlled dolostone distribution. D1 is cross-cut by stylolites, indicating that it formed before deep burial of the platform, and is observed along E–W trending normal faults which would have been open during N–S extension. Given that post-rift thermal subsidence is recorded across the Pennine Basin in the Serpukhovian (Fraser and Gawthorpe 2003), it is suggested that D1 dolomitization occurred either during or soon after deposition in the late Visean.

Zone 3 calcite cements are ubiquitous across most of the Derbyshire Platform, and also pre-date stylolitization, but are absent in D1 dolostone. This implies that dolomitization was either concurrent with, or post-dated, precipitation of this phase of calcite. Across most of the Derbyshire Platform, Zone 3 calcite cements occluded up to 70% of the interparticle pore space (Walkden and Williams 1991), thereby restricting the circulation of subsequant diagenetic fluids to faults and fractures (Hollis and Walkden 2002). Bingham (1991) noted a decrease in the volume of Zone 3 calcite towards the platform margins, however, and given the localization of D1 to the platform margins it is possible that dolomitization took place during the Serpukhovian, concurrent with Zone 3 cementation. Certainly, D1 dolomite was emplaced before reactivation of NW–SE and N–S trending faults, which host D2 and D3 dolostone, respectively, in the Bashkirian.

Three main fault trends are observed on the Derbyshire Platform, NW–SE, E–W, and N–S, with the E–W and N–S faults forming splays that originate from crustal-scale NW–SE faults (Fig. 1). Cross-cutting relationships show that E–W faults were created before the N–S trending faults, and the association of D1 dolostone with E–W faults strongly suggests that they were open during seawater circulation and D1 formation. These faults were later sealed by dolomite cement. In comparison, N–S faults host halos of a later phase of dolomite (D3) and breccias that are cemented by dolomite, galena, barite, and fluorite (Fig. 5). The cross-cutting relationship between N–S and E–W faults, along with the association of higher temperature dolostone phases and mineralization along N–S faults, is consistent with them post-dating D1 dolomitization and E–W faulting. Areas of fault interaction and intersection are often important sites for fluid flow and mineralization (Rotevatn and Bastesen 2014) and the presence of mineralized breccias and dissolution cavities at the intersection of E–W and N–S faults is consistent with this. Overall, the presence of fluorite–barite–galena–calcite assemblages in porosity in D1 dolostone, and in fractures and faults that dissect D1 and later phases of dolomitization (D2–3), is consistent with prior work, which proposed that mineralization took place as a result of basin dewatering during the

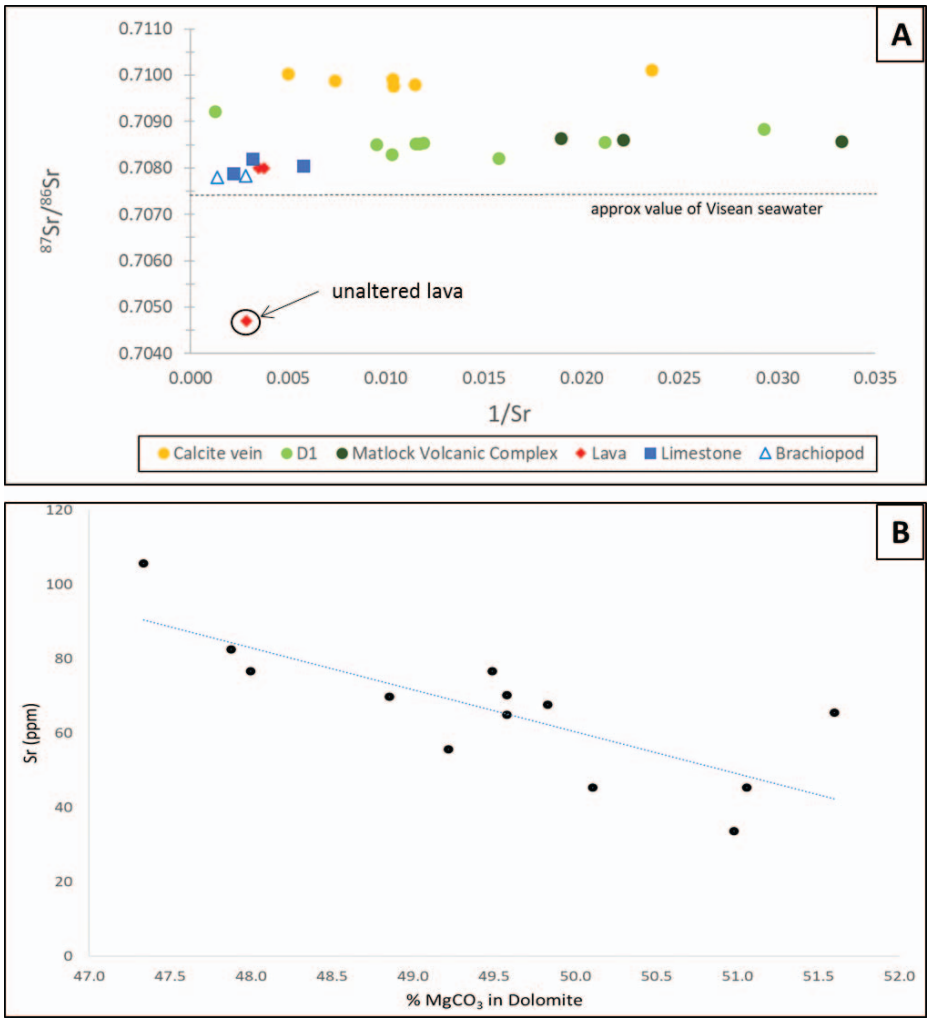

FIG. 8.—**A)** Strontium-isotope compositions of the investigated limestone, brachiopods, calcite, and dolostone samples. **B)** Dolostone Sr concentration in ppm vs. % $MgCO_3$ in dolomite. Sr concentration is seen to decrease as $MgCO_3$ content of dolomite increases.

Variscan Orogeny (Hollis and Walkden 2002 and references therein; Frazer et al. 2014).

Timing of Volcanic Alteration

Unaltered lavas sampled from Gratton Dale, located 4.5 km from the platform margin and away from D1 dolostone, have $^{87}Sr/^{86}Sr\_tr = 0.70453$, typical for basalts (Menzies and Seyfried 1979). Lavas proximal to dolomitization in the Masson Hill area, which show significant alteration, have a signature that resembles Viséan seawater (0.7078 $^{87}Sr/^{86}Sr\_tr$; Fig. 8B) suggesting that alteration took place from seawater. Identification of altered lavas within boreholes, away from the effects of surface weathering (Fig. 7A) corroborates the notion that alteration is not likely to be the result of modern surface processes. The replacement of primary iron-magnesium rich mafic minerals (olivine and pyroxene) to produce an assemblage of clay minerals, (illite, chlorite–smectite, and kaolinite), calcite, quartz, and minor pyrite is consistent with the moderate temperature (< 100 °C) alteration of the lavas via interaction with seawater and/or meteoric fluids (Lovering 1949). The high porosity in the lavas before calcite cementation would have facilitated fluid flux.

The oxygen-isotope signature of the calcite cement formed in the lava groundmass and in amygdales ($\delta^{18}O = -3‰$, n = 1) is similar to calcite precipitated from seawater; however, the $\delta^{13}C$ is isotopically lighter ($\delta^{13}C = -1.6‰$) than seawater (Fig. 9A). Assuming a mantle signature of around $\delta^{13}C = -4‰$ (Deines 2002), carbon sourced from the lavas during alteration would be isotopically depleted compared to seawater, leading to precipitation of isotopically depleted calcite cements at high fluid-rock ratios.

Dolostone Geochemistry

Calculation of the isotopic composition of the water responsible for dolomitization used Matthews and Katz (1977), assuming a fluid temperature of less than or equal to 50° C based on the presence of mono-phase fluid inclusions in D1. Viséan seawater is calculated to have $\delta^{18}O_{water} = -0.6‰$SMOW at 25° C in the study area, based on measured $\delta^{18}O_{calcite} = -3‰$, from brachiopods. The average $\delta^{18}O_{water}$ composition of the fluids responsible for dolomitization on the platform margin was calculated as $\delta^{18}O_{water} = -2.7$ ‰ SMOW (30° C), –0.6‰ SMOW (40° C), and 1.3 ‰ SMOW (50° C), using an average $\delta^{18}O_{dolomite} = -3.4\%0$, implying that the dolomitizing fluids were similar to seawater at temperatures above 40° C. Samples from the Matlock Volcanic Complex have a lighter average $\delta^{18}O_{dolomite}$ (–4.9‰ PDB) than the platform-margin, giving an estimated $\delta^{18}O_{water} = -4.2‰$ SMOW at 30° C, $\delta^{18}O_{water} = -2.1‰$ SMOW at 40° C, and –0.2‰ SMOW at 50° C (Fig. 9B). The isotopically light $\delta^{13}C$ values measured in both dolostone and calcite, precipitated in the lavas near to the Matlock Igneous Complex suggest that the carbon pool was not entirely marine, and that fluid/rock ratios were high enough to preserve the $\delta^{13}C_{water}$.

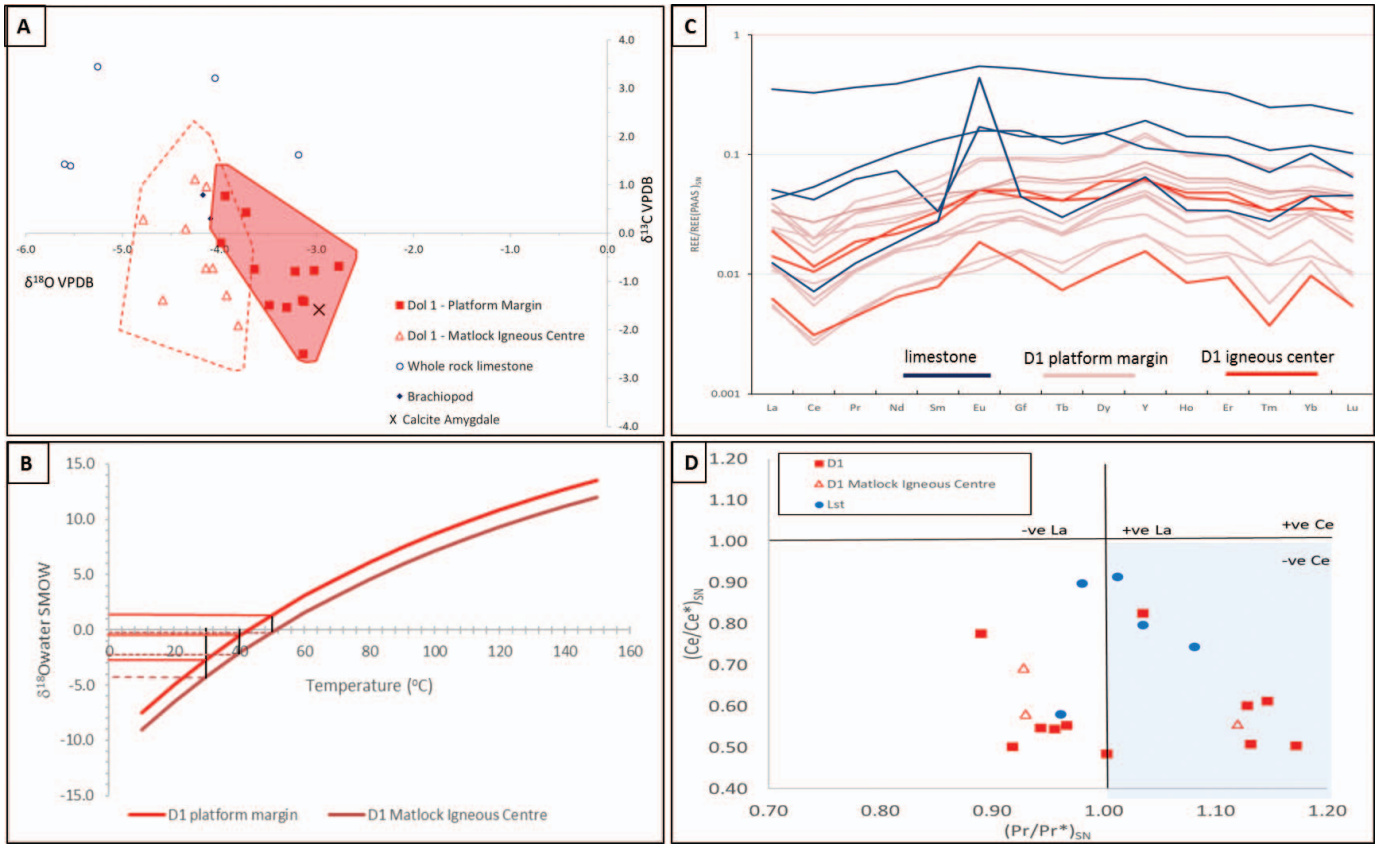

FIG. 9.—**A)** Carbon and oxygen isotope compositions of the investigated limestone, brachiopods, calcite, and dolostone samples. **B)** Calculated isotopic fluid compositional ranges for dolomitizing brine for D1 from the platform margin and Matlock Volcanic Complex, using Matthews and Katz (1977) and assuming a temperature of dolomitization between 25° C (minimum) and 50° C (maximum). **C)** REE profiles of dolostone, brachiopods, and Viséan lavas (lava data taken from Macdonald et al. 1984). **D)** Pr/Ce analysis of whole-rock dolostone and limestone samples, according to Bau and Dulksi (1996). Samples with a positive La anomaly and negative Ce anomaly, consistent with dolomitization from seawater, fall into the blue shaded area, along with most whole-rock limestones. All other values have a negative Ce and negative La anomaly, perhaps due to diagenetic modification.

The strontium-isotope composition of D1 dolostone is slightly enriched in comparison to Viséan seawater. The distribution coefficient ($D_{Sr}^{dolomite}$) for Sr in stoichiometric dolomite is 0.0118, increasing by approx. 0.0039 for each additional mol% $CaCO_3$ in non-stoichiometric dolomite (Vahrenkamp and Swart 1990). D1 dolostone is nearly stoichiometric with $MgCO_3 = 47.88$ to 51.06%, and a decrease in Sr concentration with increasing $MgCO_3$, consistent with expected behavior (Vahrenkamp and Swart 1990) (Fig. 8B). Enrichment in the $^{87}Sr/^{86}Sr$ ratio implies fluid interaction with a source of radiogenic strontium, which is usually supplied by siliciclastic minerals such as clays.

Marine carbonates inherit the REE signatures of ambient seawater, except for a slight depletion of heavy REE (HREE) (Liu et al. 2017). These REE signatures are not radically changed during dolomitization, provided that the dolomitization occurs in seawater-like fluids (Banner et al. 1988; Qing and Mountjoy 1994; Miura and Kawabe 2000; Kamber and Webb 2001; Nothdurft et al. 2004). Seawater and marine limestones generally exhibit a rare earth element (REE) profile with a marked negative Ce anomaly, but decreasing levels of oxygenation can allow greater incorporation of Ce^{3+}, removing this negative anomaly, and also leading to depletion of HREE (Hayley et al. 2004). The relatively flat REE profile, with a subtle MREE bulge, measured in D1, implies that dolomitization took place at high fluid/rock ratios either under sub-oxic conditions, at high temperature, or by interaction with another fluid. The field and paragenetic relationships, as well as petrographic and geochemical character, are inconsistent with dolomitization from a high-temperature fluid, but it is plausible that dolomitization took place beneath the sediment–water interface under sub-oxic or anoxic conditions. Comparison of normalized Pr* and Ce* values shows that although most D1 dolostones have a negative Ce and positive La anomaly, typical of seawater, some samples have a positive La anomaly (Fig. 9D), potentially reflecting sub-oxic or reducing conditions during dolomitization, post-dolomitization diagenetic overprinting, or potentially inadvertent incorporation of clay material inherent in the rock during leaching (Tostevin et al. 2016). The calculated Y/Ho ratios (35.8–51.1) are consistent with seawater (40–70; Bau and Dulski 1995), which could reflect some post-dolomitization hydrothermal modification (e.g., Ozyurt et al. 2019).

DISCUSSION

Composition of Dolomitizing Fluids

D1 dolostone reflects the first phase of dolomitization observed on the southern margin of the Derbyshire Platform. It is stratabound and variably fabric retentive with rhombic, sucrosic crystals, which are consistent with low-temperature dolomitization (Sibley and Gregg 1987). The presence of single-phase fluid inclusions suggests temperatures of up to approximately 50° C (Goldstein and Reynolds 1994). In this low-temperature setting, seawater would provide a volumetrically significant source of fluid with a sufficiently high Mg/Ca ratio for dolomitization to occur (e.g., Budd 1997; Kaczmarek and Sibley 2007; Whitaker and Xiao 2010). At temperatures of

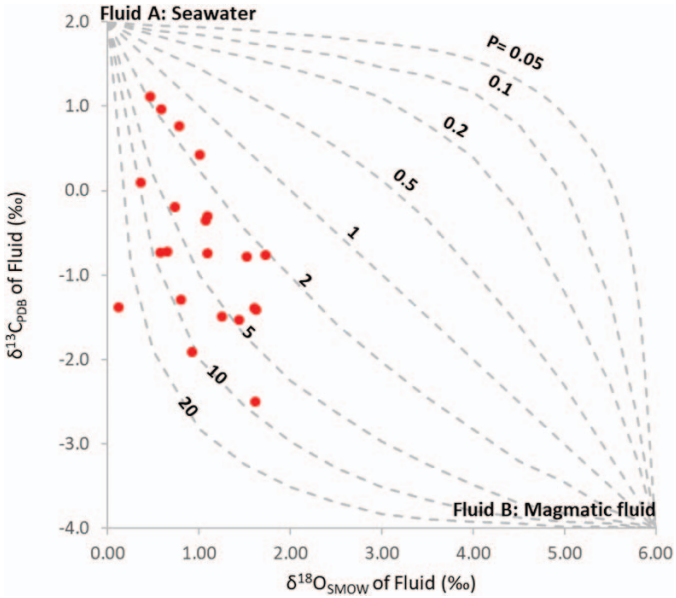

FIG. 10.—Mixing curve of fluid compositions for mixing of two fluids in $\delta^{13}C$ vs $\delta^{18}O$ space, as defined by the equations in Zheng and Hoefs (1993). Fluid B is a magmatic fluid that has a range of $\delta^{13}C = -4‰$ (PDB) and $\delta^{18}O = 6‰$ (SMOW); Fluid A is Viséan seawater $\delta^{13}C = 2‰$ (PDB) and $\delta^{18}O = 0‰$ (SMOW). P is the concentration ratio of total dissolved carbon in fluid B to that in fluid A.

50° C, the calculated $\delta^{18}O_{water}$, based on $\delta^{18}O_{dolomite}$, varies between approx. 0.2 and 1.3‰, based on the average $\delta^{18}O_{dolomite}$ of D1 dolostone from the Matlock Igneous Complex and the platform margin, respectively. This isotopic range is consistent with Carboniferous seawater (approx. 0 to –2%0; Veizer and Prokoph 2015). However, if cooler temperatures are invoked then the dolomitizing fluids must have been more isotopically depleted than seawater. This suggests either that fluid temperature was > 40° C, or that there was mixing with an isotopically lighter fluid.

Rare earth element data (Fig. 9C, D) has been interpreted to indicate dolomitization from oxic to suboxic seawater. Suboxic conditions would be consistent with dolomitization at slightly higher temperatures than ambient seawater in the shallow subsurface. The alteration of the REE profile of the whole-rock limestone during dolomitization reflects high fluid/rock ratios. Similarly, lighter $\delta^{13}C_{dolostone}$ than would be expected for Viséan seawater suggests mixing with a fluid other than seawater at high fluid/rock ratios. In order to assess this, mixing of seawater in one of two potential fluids can be considered (Fig. 10):

1. Magmatic or deep-seated crustal fluids, which have $\delta^{13}C$ values similar to the normal mantle values (from –9 to –4‰ PDB) and isotopically enriched $\delta^{18}O_{water}$ (> 0‰ SMOW)
2. Subsurface meteoric water or groundwater, with isotopically light $\delta^{18}O$ due to latitudinal and altitudinal fractionation, and isotopically light carbon due to an input of isotopically light CO_2 derived from soil processes. Walkden and Williams (1991) interpreted $\delta^{18}O_{water}$ of Serphukhovian groundwater to be as light as –6‰ from analysis of Zone 3 pore-filling calcite cements.

If dolomitization was concurrent with precipitation of Zone 3 calcite cements, then the $\delta^{18}O_{water}$ of the dolomitizing fluids could have been lowered by mixing of seawater and groundwater. Mixing with groundwater could also have lowered the $\delta^{13}C$ of the dolomitizing fluid. However, most groundwater is depleted in Mg, and fluid mixing would therefore lower the Mg/Ca ratio of the fluid, and hence reduce its dolomitizing potential. Zone 3 calcite is also only slightly isotopically depleted in carbon ($\delta^{13}C$ = approx. –0.5 to +2.5‰) due to isotopic equilibration of pore waters with limestone over the long transport distances in the aquifer (Walkden and Williams 1991), and might not therefore have reduced $\delta^{13}C_{dolomite}$.

Alternatively, the $\delta^{13}C$ of the dolomitizing fluid could have been lowered by mixing with magmatically derived CO_2. CO_2-rich waters are known to occur at the boundaries of volcanic geothermal systems and around active volcanoes (Reising and Sansone 1999) and the association between dolomitization and volcanic deposits on the southern Derbyshire Platform means that it is plausible to consider a magmatic source of CO_2. On this basis, the composition of the dolomitizing fluid was modeled using end-member fluid compositions and the general hydrothermal carbon–oxygen isotopic mixing equation from Zheng and Hoefs (1993). It was assumed that Fluid A is Viséan seawater with a composition of $\delta^{13}C = 2‰$ PDB and $\delta^{18}O = 0‰$ SMOW whilst Fluid B is mantle water with a composition of $\delta^{13}C = -4‰$ PDB and $\delta^{18}O = +6‰$ SMOW. The concentration ratio (P) of total dissolved carbon in fluid B (magmatic water) to fluid A (seawater) required to explain the isotopic composition of D1, assuming a temperature of formation of 50° C, ranges from > 20 to < 2, with most values consistent with mixing < 10 times magmatic water with seawater (Fig. 10).

Timing of Dolomitization

On the basis of oxygen-isotope and fluid-inclusion data, as well as paragenetic relationships, it would appear that formation of D1 took place in seawater. Depleted carbon-isotope ratios for some samples, beneath expected values for Carboniferous seawater ($\delta^{13}C$ +4%0; Prokoph et al. 2008), however, suggest an input of organic carbon or mixing with mantle-derived fluids. The mixing model described in the previous section suggests that seawater mixing with magmatic fluids can reasonably explain the measured $\delta^{13}C_{dolomite}$. It is likely that mantle fluids would have been present on the platform in the late Visean as a result of extrusive volcanism around the Matlock Igneous Complex. Mantle fluids may not have influenced dolomitization away from this area, and therefore such a fluid-mixing model cannot fully explain the isotopic composition of platform-margin dolostone. Furthermore, interaction of seawater and basalt leads to chlorite formation by reaction of Mg in seawater with Al and Si in the basalt during extrusive volcanism on the seafloor (Reed and Palandri 2006) and it is therefore unlikely that submarine volcanism at this time improved the dolomitizing potential of seawater. Nevertheless, reactive-transport models indicate that increased heat flow could have facilitated dolomitization across the study area (Frazer 2014).

Although carbonate sedimentation terminated on the Derbyshire Platform in the Viséan, the platform remained as a submarine ridge during the Pendleian (early Serphukhovian), becoming draped by organic-rich mudrocks as the basin underwent thermal sag subsidence (Kelling and Collinson 1992). The platform might not have been completely buried until the early Bashkerian (Collinson 1988), a period of more than 10 My after the carbonate platform drowned. As such, seawater convection could still have occurred on the platform margin and along faults. During this time, the platform underwent a series of intrusive volcanic events, leading to the emplacement of doleritic sills. The geothermal gradient on the Derbyshire Platform would have remained high, therefore, facilitating convection of seawater along the platform margin and along open faults (*sensu* Hollis et al. 2017) leading to dolomitization beneath the platform top, under suboxic conditions.

Lowenstern (2001) demonstrated that CO_2 solubility in water varies as a function of depth of volatile exsolution, and CO_2 solubility in basalts displays a prograde nature. As such, deeply sourced CO_2 would result in the generation of acidity towards the surface, and therefore mixing of seawater and even a small volume of mantle-derived fluids could have lowered the pH of the fluid, as well as its $\delta^{13}C$. The increased acidity would have increased the rate of dissolution of mafic minerals, such as olivine and

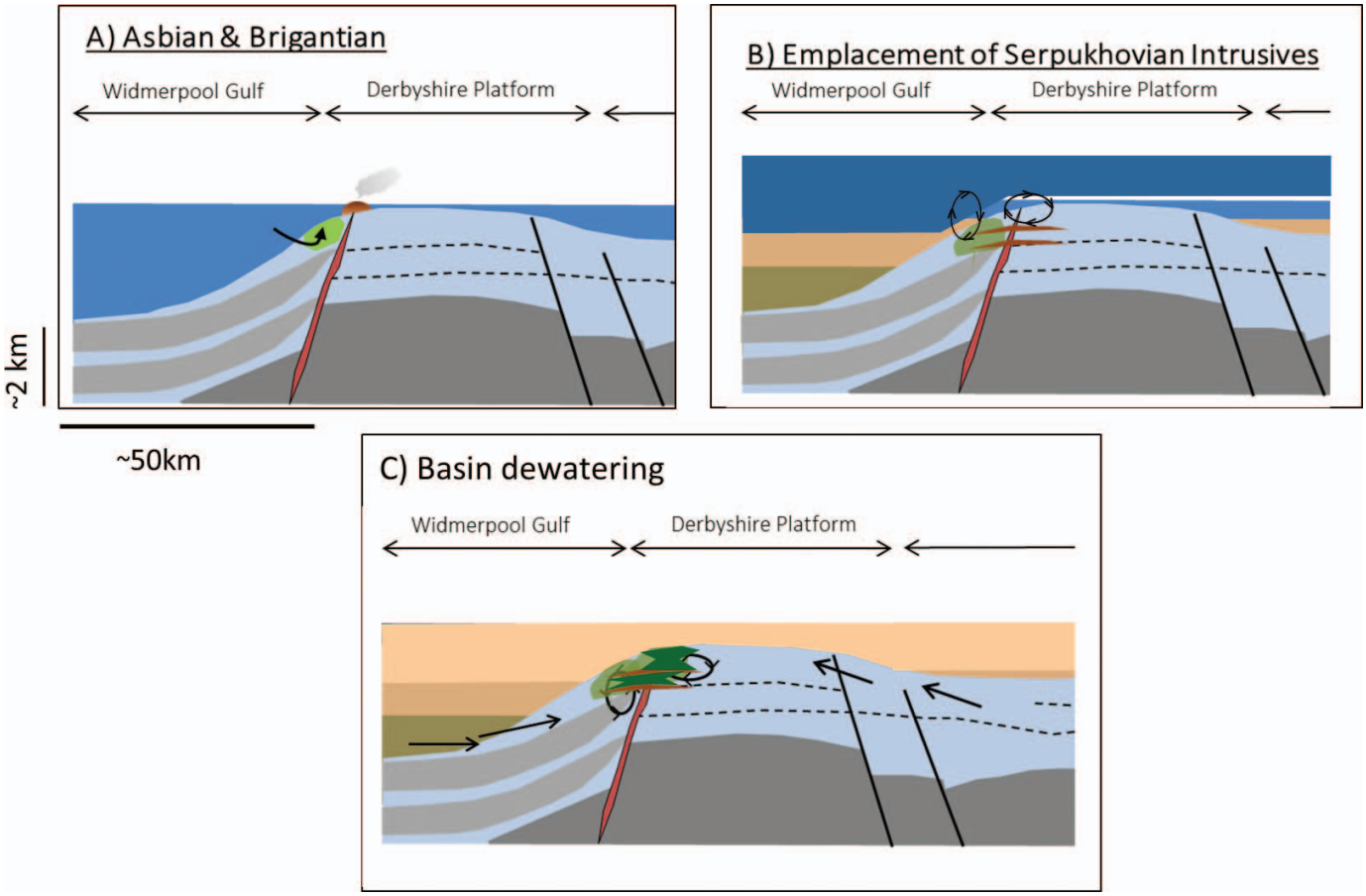

FIG. 11.—Conceptual model of dolomitisation on the Derbyshire Platform. **A)** During the Asbian and Brigantian, seawater convected through the porous and permeable platform margin facies, driven by a high geothermal gradient. **B)** By the early Serphukovian, the platform had drowned and sills were emplaced. Seawater continued to convect on the platform margin and along faults, with leaching of Mg from interbedded volcanics facilitated by a decrease in pH from mantle-derived CO_2. At the same time, groundwater fluxed eastwards under gravity, across the East Midlands Shelf (Walkden and Williams 1991). **C)** Dolomitization from seawater waned as the platform was buried during the Serphukhovian. Once the platform was buried beneath shales, compactional dewatering and seismically-driven fluid expulsion (Frazer et al. 2014) led to dolomitization along faults (D2), overprinting D1 dolomite.

pyroxene (Reising and Sansone 1999; Robinson et al. 2019) in the basalts that are interbedded with dolostone in the vicinity of the Matlock Igneous Complex. As a result, Mg would have been released through carbonation of interbedded basalts, increasing the Mg/Ca ratio of the fluid and also liberating silica (Robertson et al. 2019; Koeshidayatullah et al. 2020). The association of dolomitization, volcanism, and silicification of limestone in the vicinity of the Matlock Igneous Complex can consequently be explained by this process. The interpretation is supported by strontium-isotope data; unaltered lavas sampled from Gratton Dale, located 4.5 km from the platform margin and not associated with dolomitization, have a depleted strontium signature of $^{87}Sr/^{86}Sr\_tr$ 0.70453, typical of basalts (Menzies and Seyfried 1979). Conversely, altered lavas in the vicinity of dolostone have signatures that resemble Viséan seawater (0.7078 $^{87}Sr/^{86}Sr\_tr$). The cause of enrichment of radiogenic strontium in D1 dolostone is not entirely clear, but it is possible that it reflects an increase in clay content in the basin, with deposition of mudrocks in the deepest part of the basin from the earliest Serpukhovian. This might also have led to some minor clay contamination in samples that is also reflected in the REE results (see Tostevein et al. 2016).

The REE signature of D1 dolostone is interpreted to reflect varying degrees of oxygenation of the dolomitizing fluid. However, mixing with magmatic fluids under high water/rock ratios could also have altered the REE composition of the resultant dolostone (Murray et al. 1991; Webb and Kamber 2000; Shields and Stille 2001; Nothdurft et al. 2004; Webb et al. 2009; Liu et al. 2017). REEs can be mobilized during hydrothermal alteration (Taylor and Fryer 1980; Palacios et al. 1986; Fulignati et al. 1999), particularly during the interaction between seawater and mafic volcanics (Frey et al. 1977; Wood et al. 1976; Hellman and Henderson 1977; Ludden and Thompson 1979) and this could have led to the observed depletion in the HREEs, creating a slight MREE bulge. This alteration would also have depleted Y concentrations, lowering the Y/Ho ratio.

Conceptual Model of Diagenetic Fluid Flow and Dolomitization

Dolomitization on the southern margin of the Derbyshire Platform is broadly stratabound and occurs in platform-margin facies, along E–W faults, and close to lavas in the Matlock Igneous Complex. The association of the dolostone with E–W faults indicates that these faults were open during seawater circulation and formation of D1 dolostone. The fabric and texture of the dolostone, along with primary monophase fluid inclusions, indicate formation at temperatures up to 50° C. During the Viséan (Fig. 11A) and the Serphukhovian (Fig. 11B), until the platform was draped by onlapping clastic sediments, geothermal convection could have occurred along the platform margin and also along E–W faults, driven by the temperature differential between the cooler seawater in the Widmerpool

Basin and the warmer, volcanically active platform top (Frazer et al. 2014; Frazer 2014). Within the vicinity of the Matlock Igneous Complex, interaction of seawater with submarine basalts that were extruded onto the seafloor could have removed Mg from seawater (Reed and Palandri 2006), however, reducing the dolomitizing potential of seawater in the vicinity of lava extruded during carbonate-platform growth. Consequently, dolomitization may only have occurred initially on the platform margin, and along E–W faults, perhaps facilitated by the increased heat flux associated with volcanic activity. Nevertheless, the preservation of olivine in some basalts suggests that serpentinization was not pervasive, and that the diagenetic potential of the lavas remained high.

With the onset of post-rift thermal subsidence in the Serpukhovian, the Derbyshire Platform was drowned and the surrounding hanging-wall basins accumulated fine-grained mudrocks (Fig. 11B). During this time, gravity-driven meteoric fluids flowed westwards from the East Midlands Platform, eventually leading to porosity occlusion by calcite cement phase Zone 3 on the Derbyshire Platform, but decreasing in volume towards the platform margin (Bingham 1991; Walkden and Williams 1991). At the same time, volcanism changed from extrusive to intrusive, leading to emplacement of doleritic sills (Macdonald et al. 1984). This would have facilitated dolomitization by maintaining a high heat flow and by increasing pCO_2 (e.g., Sibley 1990). Furthermore, CO_2 degassing would have lowered the pH of fluids, allowing magnesium to be leached from olivine and pyroxene in basalts, increasing the Mg/Ca ratio of the fluid (e.g., Robertson et al. 2019; Koeshidayatullah et al. 2020). Alteration of the basalts would also have released silica, implying a genetic link between the occurrence of dolostone the occurrence of silicified limestones close to the igneous intrusive sills and extrusive lavas, parallel to E–W oriented faults.

Once dolomitization was complete, dolomite cements precipitated along, and sealed E–W trending faults. There was also cementation of the extrusive lavas by calcite, such that later diagenetic fluids could not exploit the same fluid pathways as the dolomitizing fluids that formed phase D1. Support for this model comes from both the geochemical fingerprint of the dolostone and the localized silicification observed in the vicinity of the Matlock igneous center, since quartz is a by-product of the carbonation of ultramafic rocks (Lovering 1949). By the Bashkerian, the platform was buried underneath upper Carboniferous sediments (Collinson 1988), which became overpressured until the onset of the Variscan Orogeny led to rupture and fluid expulsion (Frazer et al. 2014). At this point, dolomitizing fluids were expelled along faults, leading to the formation of D2 dolostone along the Cronkston–Bonsall Fault, probably overprinting precursor D1 dolostone (Fig. 11C).

Implications to Dolomitization Within Extensional Basins

In the Pennine Basin, dolomitization commonly occurs on the margins of age-equivalent carbonate platforms, formed under the same tectono-stratigraphic regime (e.g., Bouch et al. 2004; Hollis and Walkden 2012; Juerges et al. 2016), often at zones of fault intersection or termination (Fig. 1). This is consistent with observations from the Suez rift, where fault-controlled dolomitization occurs in zones of structural complexity (e.g., Hollis et al. 2017; Hirani et al. 2018). However, the volume of dolostone at other localities in the Pennine Basin is significantly less than on the Derbyshire Platform, with body sizes typically less than 20 km^2. They are also not associated with igneous activity; volcanism in the Pennine Basin in the Carboniferous was restricted to the Derbyshire Platform. From field and petrographical data, it is estimated that up to 50% of the dolostone mapped on the southern Derbyshire Platform was formed from modified seawater during the Visean and Serpukhovian, i.e., potentially > 25 km^2, whereas the remainder formed from basinal brines expelled from juxtaposed hanging-wall basins (Frazer et al. 2014).

Where D1 dolostone has not been recrystallized, it has a well-connected intercrystalline pore network (Fig. 6A), indicating that the petrophysical properties of limestone can be positively affected by dolomitization through geothermal convection of seawater. Consequently, the potential for these dolostones to host mineralization, hydrocarbons, or groundwater is high. For the same reason, the ability to flux subsequent diagenetic fluids was also improved. D1 dolomite crystals could have nucleated subsequent phases of dolomitization. On the Derbyshire Platform, later dolomitization events occurred along NW–SE and N–S trending faults, thus producing phases D2–D5 which cross-cut D1. This suggests that the presence of a large area of dolomitization on the platform could have been a vital template for subsequent phases of dolomitization in the area, enlarging the volume of dolostone to > 60 km^2 (Breislin 2018).

Globally, carbonate platforms commonly form on the footwalls of normal faults in extensional basins (Bosence 2012). The coincidence of active tectonism, high heat flow, seawater, and volcanic activity in these basins means that dolomitization from geothermal convection of seawater that has interacted with magmatic fluids should be common, as suggested by some well-documented case studies (e.g., Nader et al. 200; Blomme et al. 2017; Jacquemyn et al. 2017). On the Latemar Platform, for example, dolomitization is interpreted to be the product of seawater interaction with mafic dikes, forming dolostone halos (0.5 to 2.5 m wide) (e.g., Zheng 1990; Carmichael and Ferry 2008; Blomme et al. 2017; Jacquemyn et al. 2017). In the Levant region of Lebanon, hydrothermal dolomitization ($T_H = 50–80°$ C) has been related to volcanism in the Late Jurassic, which created a locally high geothermal gradient, optimizing the thermodynamic and kinetic potential for dolomitization (Nader et al. 2004). There are not many case studies, however, perhaps for several reasons. Firstly, dolomitization in extensional basins might have been attributed to hydrothermal processes, particularly where dolostone forms along faults, without a full explanation of the potential source of the fluids. This could reflect three scenarios. 1) The generic assumption that dolomitization was from upward-flowing, crustal fluids—often invoked for hydrothermal dolomitization (e.g., Davies and Smith 2006 and discussion in Hollis et al. 2017). 2) An indirect control of extensional tectonics on dolomitization, through an increase in the geothermal gradient. In this case, high heat flow might have facilitated dolomitization, but might not be recognized geochemically. This would be also be the case if there were low volumes of fluid mixing with seawater, such that the REE and/or isotopic signature of the dolomitizing brine was not altered by fluid mixing. 3) Recrystallization of the earliest phase of dolomite, with hotter, more saline brines. Alternatively, the coincidence of a CO_2-rich brine, circulating through mafic or ultramafic rocks, adjacent to permeable carbonate strata, might be rare. In this case, dolomitization by the process invoked in this study might be uncommon. In order to test the model, evaluation of dolomitization processes in rift basins with widespread carbonate sedimentation, could be critical to assessing the wider occurrence of dolomitization by convection of mixed seawater and magmatic water. The observations made in this study could also go some way to explain the commonly observed association of replacive silica in fault-controlled dolostones in extensional basins.

CONCLUSIONS

Based on the data presented, the following conclusions have been drawn:

- Dolomitization of the Derbyshire Platform was a multi-phase event, with the earliest dolostone phase, D1, accounting for approximately 50% of the total dolostone volume (approx. 25 km^2 of a total of 60 km^2 of dolostone on the platform).
- D1 dolostone is stratabound and facies controlled and occurs in platform margin facies, close to interbedded basaltic lavas around the Matlock Volcanic Complex.

- D1 dolostone is fabric retentive, composed of buff-gray, clean planar-e crystals. It is cross-cut by stylolites, and primary fluid inclusions are predominantly monophase, indicating formation at shallow burial depths and temperatures $< 50°$ C.
- Geochemical evidence points towards early dolomitization from seawater that circulated on the platform margin and syn-rift, E–W trending faults in the Viséan, which became progressively modified, through mixing with mantle-derived CO_2, in the Serpukhovian, during platform drowning.
- The addition of CO_2 to circulating seawater lowered the pH of the brine, leading to carbonation of interbedded basalts. This resulted in calcite cementation of vesicles and an increase in the Mg/Ca ratio of the fluid, which may have further facilitated dolomitization. Concomitant release of silica during this process also led to localized areas of silicification close to the Matlock Volcanic Complex.
- This model could account for variability in the occurrence of dolomite on carbonate platforms in rift basins, with larger and more pervasive zones of dolomite occurring where there is alteration of underlying or interbedded mafic rocks.

ACKNOWLEDGMENTS

Catherine Breislin gratefully acknowledges funding by Natural Environment Research Council Doctoral Training Programme grant number NE/L002469/1 with CASE support by Shell International Exploration and Production and the British Geological Survey. The authors thank Jon Fellows and John Waters at The University of Manchester and James Utley at The University of Liverpool for analytical services provided. The British Geological Survey is thanked for the loan of material. VJB, IM, and JBR publish with the approval of the Chief Executive Officer, British Geological Survey (NERC). Sarah Newport (University of Manchester) and Dr. Richard Shaw are thanked for their field assistance. Alanna Juerges, Conxita Taberner, and the Carbonate Research team at Shell International Exploration and Production and Hamish Robertson, University of Bristol, are thanked for their helpful discussions. The comments of two anonymous reviewers and Associate Editor Stephen Kaczmarek and Chief Editor Peter Burgess greatly improved a previous version of this paper.

REFERENCES

Aitkenhead, N., and Chisholm, J., 1982, A standard nomenclature for the Dinantian formation of the Peak longitudinal and District of Derbyshire and Staffordshire: Institute of Geology, Report 8, 17 p.

Aitkenhead, N., Chisholm, J.I., and Stevenson, I.P., 1985, Geology of the country around Buxton, Leek and Bakewell: British Geological Survey, Memoir, Sheet 111, 168 p.

Alderton, D.H.M., and Bevins, E., 1996, P-T conditions in the South Wales Coalfield: evidence from coexisting hydrocarbon and aqueous fluid inclusions: Geological Society of London, Journal, v. 153, p. 265–275.

Banner, J.L., Hanson, G.N., and Meyers, W.J., 1988, Rare earth element and Nd isotopic variations in regionally extensive dolomites from the Burlington, Keokuk Formation (Mississippian): implications for REE mobility during carbonate diagenesis: Journal of Sedimentary Petrology, v. 58, p. 415–432.

Bau, M., and Dulski, P., 1995, Comparative study of yttrium and rare-earth element behaviours in fluorine-rich hydrothermal fluids: Contributions to Mineralogy and Petrology, v. 119, p. 213–223.

Bau, M., and Dulski, P., 1996, Distribution of yttrium and rare-earth elements in the Penge and Kuruman iron formations, Transvaal Supergroup, South Africa: Precambrian Research, v. 79, p. 37–55.

Bingham, G.C., 1991, The origin and interaction of diagenetic fluids in the Derbyshire–East Midland Shelf [Ph.D. Thesis]: University of Aberdeen, 325 p.

Blomme, K., Fowler, S.J., Bachaud, P., Nader, F.H., Michel, A., and Swennen, R., 2017, Ferroan dolomitization by seawater interaction with mafic igneous dikes and carbonate host rock at the Latemar platform, dolomites, Italy: numerical modelling of spatial, temporal, and temperature data: Geofluids, v. 2017, p. 1–14.

Bosence, D.W.J., 2012, Carbonate-dominated marine rifts, *in* Roberts, D.G., and Bally, A.W., eds., Phanerozoic Rift Systems and Sedimentary Basins: Elsevier, p. 104–130.

Bouch, J.E., Milodowski, A.E., and Ambrose, K., 2004, Contrasting patterns of pore-system modification due to dolomitization and fracturing in Dinantian basin-margin carbonates from the UK, *in* Braithwaite, C.J.R., Rlzm, G., and Darke, G., eds., The Geometry and Petrogenesis of Dolomite Hydrocarbon Reservoirs: Geological Society of London, Special Publication 235, p. 325–348.

Breislin, C.J., 2018, Basin-Scale Mineral and Fluid Processes at a Platform Margin, Lower Carboniferous, UK [Ph.D. Thesis]: University of Manchester, 236 p.

Budd, D.A., 1997, Cenozoic dolomites of carbonate islands: their attributes and origin: Earth Science Reviews. v. 42, p. 1–47.

Burke, W.H., Denison, R.E., Hetherington, E.A., Koepnick, R.B., Nelson, H.F., and Otto, J.B., 1982, Variation of seawater $^{87}Sr/^{86}Sr$ throughout Phanerozoic time: Geology, v. 10, p. 516–519.

Carmichael, S.K., and Ferry, J.M., 2008, Formation of replacement dolomite in the Latemar carbonate buildup, Dolomites, northern Italy: Part 2. Origin of the dolomitizing fluid and the amount and duration of fluid flow: American Journal of Science, v. 308, p. 885–904.

Charlier, B.L.A., Ginibre, C., Morgan, D., Nowell, G.M., Pearson, D.G., Davidson, J.P., and Ottley, C.J., 2006, Methods for the microsampling and high-precision analysis of strontium and rubidium isotopes at single crystal scale for petrological and geochronological applications: Chemical Geology, v. 232, p. 114–133.

Chisholm, J., Mitchell, M., Strank, A., Cox, F., and Harrison, D., 1983, A revision of the stratigraphy of the Asbian and Brigantian limestones west of Matlock: Institute of Geological Sciences, Report 83, 1724 p.

Chisholm, J.I., Charsley, T.J., and Aitkenhead, N., 1988, Geology of the country around Ashbourne and Cheadle: British Geological Survey, Memoir, Sheet 124.

Chisholm, J., and Butcher, N., 1981, Limestone on top of dolomite in a recent borehole near cromford: Mercian Geologist, v. 8, p. 225–228.

Coleman, T.B., Jones, D.G., Plant, J.A., and Smith, K., 1989, Metallogenic models for carbonate-hosted (Pennine and Irish-style) mineral deposits, *in* Plant, J.A., and Jones, D.G., eds., Metallogenic Models and Exploration Criteria for Buried Carbonate-Hosted Ore Deposits: a Multidisciplinary Study in Eastern England: London, Keyworth and Institute of Mining and Metallurgy, British Geological Survey, p. 123–134.

Collinson, J.D., 1988, Controls on Namurian sedimentation in the central province basins of Northern England, *in* Besley, B.M., and Kelling, G., eds., Sedimentation in a Synorogenic Basin Complex: The Upper Carboniferous of NW Europe: London, Blackie, p. 85–101.

Cope, F.W., 1973, Woo Dale borehole near Buxton, Derbyshire: Nature Physical Science, v. 243, p. 29–30.

Deines, P., 2002, The carbon isotope geochemistry of mantle xenoliths: Earth-Science Reviews, v. 58, p. 247–278.

Deniel, C., and Pin, C., 2001, Single-stage method for the simultaneous isolation of lead and strontium from silicate samples for isotopic measurements: Analytica Chimica Acta, v. 426, p. 95–103.

Dunham, K.C., 1952, Fluorspar, Fourth Edition: British Geological Survey, Mineral Resources, Memoir 4, p. 162.

Dunham, K.C., 1983, Ore genesis in the English Pennines: a fluorite subtype, *in* Kisvar-Sanyi, G., Grant, S.K., Pratt, W.P., and Koenig, J.W., eds., International Conference on MVT Lead-Zinc Deposits, Proceedings: Rolla, University of Missouri Press, p. 86–112.

Floyd, P.A., and Winchester J.A., 1975, Magma types and tectonic setting discrimination using immobile elements: Earth and Planetary Science Letters. v. 27, p. 211–218.

Ford, T.D., 2001, The geology of the Matlock mines: a review: Mining History: Peak District Mines Historical Society, Bulletin, v. 14, p. 61–92.

Ford, T.D., 2002, Dolomitization of the carboniferous limestone of the Peak District: a review: Mercian Geologist, v. 15, p. 163–170.

Ford, T., and Quirk, D., 1995, Mineralization of the south Pennines: Geology Today, v. 11, 77 p.

Fowles, J., 1987, Dolomitisation of the Derbyshire Platform [Ph.D. Thesis]: University of Cambridge, Cambridge, U.K.

Fraser, A., and Gawthorpe, R.L., 1990, Tectono-stratigraphic and hydrocarbon habitat of the Carboniferous in northern England, *in* Hardman, R., and Brooks, J., eds., Tectonic Events Responsible for Britain's Oil and Gas Reserves: Geological Society of London, Special Publication 55, p. 49–86.

Fraser, A.J., and Gawthorpe, R.L., 2003, An atlas of Carboniferous basin evolution in Northern England: Geological Society of London, Memoir 28, 70 p.

Frazer, M., 2014, Advances in understanding the evolution of diagenesis in Carboniferous carbonate platforms: insights from simulations of palaeohydrology, geochemistry, and stratigraphic development [Ph.D. Thesis]: University of Manchester, 261 p.

Frazer, M., Whitaker, F., and Hollis, C., 2014, Fluid expulsion from overpressured basins: implications for Pb-Zn mineralisation and dolomitization of the East Midlands platform, northern England: Marine and Petroleum Geology, v. 55, p. 68–86.

Frey, F.A., Green, D.H., and Koy, S.D., 1977, Integrated models of basalt petrogenesis: a study of quartz tholeiites to olivine melilitites from south eastern Australia utilizing geochemical and experimental petrological data: Journal of Petrology, v. 19, p. 463–513.

Friedman, I., and O'Neil, J.R., 1977, Compilation of stable-isotope fractionation factors of geochemical interest, *in* Fleischer, M., ed., Data of Geochemistry: U.S. Geological Survey, Professional Paper 440KK, 12 p.

Fulignati, P., Gioncada, A., and Sabrana, A., 1999, Rare-earth element (REE) behaviour in the alteration facies of the active magmatic-hydrothermal system of Volcano (Aeolian Islands, Italy): Journal of Volcanology and Geothermal Research, v. 88, p. 325–342.

Gawthorpe, R.L., 1987, Tectono-sedimentary evolution of the Bowland Basin, N England, during the Dinantian: Geological Society of London, Journal, v. 144. p. 59–71.

Goldstein, R.H., and Reynolds, T.J., 1994, Systematics of Fluid Inclusions in Diagenetic Minerals: SEPM, Short Course 31, 199 p.

Gradstein, F., and James, O., 2004, Geologic Time Scale 2004: why, how, and where next!: Lethaia, v. 37, p. 175–181.

Guion, P.D., and Fielding, C.R., 1988, Westphalian A and B sedimentation, *in* Besley, B.M., and Kelling, G., eds., Sedimentation in a Synorogenic Basin Complex: the Upper Carboniferous of NW Europe: Glasgow, Blackie, p. 153–177.

Gutteridge, P., 1987, Dinantian sedimentation and the basement structure of the Derbyshire Dome: Geological Journal, v. 22, p. 25–41.

Gutteridge, P., 1991, Aspects of Dinantian sedimentation in the Edale Basin, North Derbyshire: Geological Journal, v. 26, p. 245–269.

Hayley, B.A., Klinkhammer, G.P., and McManus, J., 2004., Rare earth elements in pore waters of marine sediments: Geochimica et Cosmochimica Acta, v. 68, p. 1265–1279.

Hellman, P., and Henderson, P., 1977, Are rare earth elements mobile during spilitisation?: Nature, v. 267, p. 38–40.

Hirani, J., Bastesen, E., Boyce, A., Corlett, H., Eker, A., Gawthorpe, R., Hollis, C., Korneva, I., and Rotevatn, A., 2018, Structural controls on non-fabric-selective dolomitization within rift-related basin-bounding normal fault systems: insights from the Hammam Faraun Fault, Gulf of Suez, Egypt: Basin Research, v. 30, p. 990–1014.

Hollis, C., 1998, Reconstructing fluid history: an integrated approach to timing fluid expulsion and migration on the Carboniferous Derbyshire Platform, England, *in* Parmell, J., ed., Dating and Duration of Fluid Flow and Fluid-Rock Interaction: Geological Society of London, Special Publication 144, p. 153–159.

Hollis, C., and Walkden, G., 1996, Use of burial diagenetic calcite cements to determine the controls upon hydrocarbon emplacement and mineralization on a carbonate platform, Derbyshire, England: Geological Society of London, Special Publication 391, p. 107–127.

Hollis, C., and Walkden, G., 2002, Reconstructing fluid expulsion and migration north of the Variscan Orogen, Northern England: Journal of Sedimentary Research, v. 64, p. 134–165.

Hollis, C., and Walkden, G., 2012, Burial diagenetic evolution of the Lower Carboniferous (Dinantian) of the southern margin of the Askrigg Platform and a comparison with the Derbyshire Platform: Petroleum Geoscience, v. 18, p. 83–95.

Hollis, C., Bastesen, E., Boyce, A., Corlett, H., Gawthorpe, R., Hirani, J., and Whitaker, F., 2017, Fault controlled dolomitization in a rift basin: Geology, v. 45, p. 219–222.

Hurt, L., 1968, A report on Nestus Mine and other shafts on the Heights of Abraham, Matlock Bath, Derbyshire: Peak District Mines Historical Society, Bulletin, v. 3, p. 369–379.

Ixer, R.A., 1975, A revision of part of the Matlock Group at Masson Hill, Matlock: Mercian Geologist, v. 5, p. 181–188.

Ixer, R.A., 1978, The emplacement of a fluorspar flat at Masson Hill, Matlock, Derbyshire: Mercian Geologist, v. 6, p. 245–255.

Ixer, R.A., and Vaughan, D.J., 1993, Lead–zinc–fluorite–barite deposits of the Pennines, North Wales and the Mendips, *in* Pattrick, R.A.D., and Polya, D.A., eds., Mineralization in the British Isles: London, Chapman and Hall, p. 55–411.

Jacquemyn, C., El Desouky, H., Hunt, D., Casini, G., and Swennen, R., 2001, Dolomitization of the Latemar platform: fluid flow and dolomite evolution: Marine and Petroleum Geology, v. 55, p. 43–67.

Jones, B., Luth, R.W., and MacNeil, A.J., 2001, Powder X-ray diffraction analysis of homogenous and heterogeneous sedimentary dolostones: Journal of Sedimentary Research, v. 71, p. 790–799.

Juerges, A., Hollis, C.E., Marshall, J., and Crowley, S., 2016, The control of basin evolution on patterns of sedimentation and diagenesis: an example from the Mississippian Great Orme, North Wales: Geological Society of London, Journal, v. 173, p. 438–456.

Kaczmarek, S.E., and Sibley, D.F., 2007, A comparison of nanometer-scale growth and dissolution features on natural and synthetic dolomite crystals: implications for the origin of dolomite: Journal of Sedimentary Research, v. 77, p. 424–435.

Kamber, B.S., and Webb, G.E., 2001, The geochemistry of late Archaean microbial carbonate: implications for ocean chemistry and continental erosion history: Geochimica et Cosmochimica Acta, v. 65, p. 2509–2525.

Kelling, G., and Collinson, J.D., 1992, Silesian, *in* Duff, P., and Smith, A., eds., The Geology of England and Wales: Geological Society of London, v. 87, p. 239–263.

Koeshidayatullah, A., Corlett, H., Stacey, J., Swart, P.K., Boyce, A., Robertson, H., Whitaker, F., and Hollis, C., 2020, Evaluating new fault-controlled hydrothermal dolomitisation models: insights from the Cambrian Dolomite, Western Canadian Sedimentary Basin: Sedimentology, doi:10.1111/sed.12729.

Lavoie, D., Chi, G., Urbatsch, M., and Davis, W., 2010, Massive dolomitization of a pinnacle reef in the Lower Devonian West Point Formation (Gaspe Peninsula, Quebec): an extreme case of hydrothermal dolomitization through fault-focused circulation of magmatic fluids: American Association of Petroleum Geologists, Bulletin, v. 94, p. 513–531.

Lavoie, D., Rivard, C., Lefebvre, R., Séjourné, S., Thériault, R., Duchesne, M., Ahad, J., Wang, B., Benoit, N., and Lamontagne, C., 2014, The Utica Shale and gas play in southern Quebec: geological and hydrogeological syntheses and methodological approaches to groundwater risk and evaluation: International Journal of Coal Geology, v. 126, p. 77–91.

Liu, J., Zheng, H., Liu, B., Hongguang, L., Shi, K., Rongtao, G., and Zhang, X., 2017, Petrology and geochemical characteristics of dolomite in the Middle Permian Maoukou Formation, central Sichuan: Petroleum Research, v. 2, p. 366–377.

Lovering, M., 1949, Rock alteration as a guide to ore: east Tintic District, Utah: Economic Geology, Monograph 1, 64 p.

Lowenstern, J.B., 2001, Carbon dioxide in magmas and implications for hydrothermal systems: Mineralium Deposita, v. 36, p. 490–502.

Ludden, J.M., and Thompson, G., 1979, An evaluation of the behavior of the rare earth elements during weathering of seafloor basalt: Earth and Planetary Science Letters, v. 43, p. 85–92.

Macdonald, R., Gass, K., Thorpe, I., and Gass, G., 1984, Geochemistry and petrogenesis of the Derbyshire Carboniferous Basalts: Geological Society of London, Journal, v. 141, p. 147–159.

Matthews, A., and Katz, A., 1977, Oxygen isotope fractionation during the dolomitization of calcium carbonate: Geochimica et Cosmochimica Acta, v. 41, p. 1431–1438.

McCrea, J.M., 1950, On the isotope chemistry of carbonate and a palaeotemperature scale: Journal of Physical Chemistry, v. 18, 726 p.

McKenzie, D.P., 1978, Some remarks on the development of sedimentary basins: Earth and Planetary Science Letters, v. 40, p. 25–32.

Menzies, M., and Seyfried, W., 1979, Basalt–seawater interaction trace element and strontium isotope variations in experimentally altered glassy basalt: Earth and Planetary Science Letters, v. 44, p. 463–472.

Miura, N., and Kawabe, I., 2000, Dolomitization of limestone with $MgCl_2$ solution at 150°C: preserved original signatures of rare earth elements and yttrium as marine limestone: Geochemical Journal, v. 34, p. 223–227.

Murray, R.W, Buchholtz ten Brink, M.R, Gerlach, D.C., and Russell, G.P., 1991, Rare earth, major, and trace elements in chert from the Franciscan Complex and Monterey Group, California: assessing REE sources to fine-grained marine sediments: Geochimica et Cosmochimica Acta, v. 55, p. 1875–1895.

Nader, F., Swennen, R., and Ellam, R., 2004, Field geometry, petrography and geochemistry of a dolomitization front (Late Jurassic, central Lebanon): Sedimentology, v. 54, p. 1093–1120.

Nance, W.B., and Taylor, S.R., 1976, Rare earth element patterns and crustal evolution-l. Australian post-Archean sedimentary rocks: Geochimica et Cosmochimica Acta, v. 40, p. 1539–1551.

Nothdurft, L.D., Webb, G.E., and Kamber, B.S., 2004, Rare earth element geochemistry of Late Devonian reefal carbonates, Canning Basin, Western Australia: confirmation of a seawater REE proxy in ancient limestones: Geochimica et Cosmochimica Acta, v. 68, p. 263–283.

Ozyurt, M., Kiraci, M.Z., and A-Aasm, I.S., 2019, Geochemical characteristics of Upper Jurassic–Lower Cretaceous platform carbonates in Hazine Magˇ ara, Gümüşhane (northeast Turkey): implications for dolomitization and recrystallization: Canadian Journal of Earth Sciences, v. 56, p. 306–320.

Palacios, C.M., Hein, U.F., and Dulski, P., 1986, Behaviour of rare earth elements during hydrothermal alteration at the Buena Esperanza copper–silver deposit, northern Chile: Earth and Planetary Science Letters, v. 80, p. 208–216.

Pearce, J.A., and Cann. J.R. 1973, Tectonic setting of basic volcanic rocks determined by using trace element analyses: Earth and Planetary Science Letters, v. 19, p. 290–300.

Pearce, J.A., and Norry, M.J., 1979, Petrogenetic implications of Ti, Zr, Y and Nb variations in volcanic rocks: Contributions to Mineralogy and Petrology, v. 69, p. 33–47.

Pollington, A.D., and Baxter, E.F., 2010, High resolution Sm–Nd garnet geochronology reveals the uneven pace of tectono-metamorphic processes: Earth and Planetary Science Letters, v. 293, p. 63–71.

Prokoph, A., Shields, G., and Veizer, J., 2008, Compilation and time-series analysis of a marine carbonate $\delta^{18}O$, $\delta^{13}C$, $^{87}Sr/^{86}Sr$ and $\delta^{34}S$ database through Earth History: Earth Science Reviews, v. 87, p. 113–133.

Qing, H., and Mountjoy E.W., 1994, Formation of coarsely crystalline, hydrothermal dolomite reservoirs in the Presqu'ile barrier, Western Canada Sedimentary Basin: American Association of Petroleum Geologists, Bulletin, v. 78, p. 55–77.

Reed, M.H., and Palandri, J., 2006, Sulfide mineral precipitation from hydrothermal fluids, *in* Vaughan, D.J., ed., Sulfide Mineralogy and Geochemistry: Mineralogical Society of America, Reviews in Mineralogy and Geochemistry, v. 61, p. 609–631.

Reising J., and Sansone, J., 1999, The chemistry of lava–seawater interactions: the generation of acidity: Geochemica et Cosmochimica Acta, v. 63, p. 2183–2196.

Robertson, H., Corlett, H., Hollis, C., Kibblewhite, T., and Whitaker, F. 2019, Listwanitization as a source of Mg for dolomitization: field evaluation in Atlin, British Columbia [Abstract]: Goldschmidt Conference, August 2019, Barcelona.

Rotevatn, A., and Bastesen, E., 2014, Fault linkage and damage zone architecture in tight carbonate rocks in the Suez Rift (Egypt): implications for permeability structure along segmented normal faults, *in* Spence, G.H., Redfern, J., Aguilera, R., Bevan, T.G., Cosgrove, J.W., Couples, G.D., and Daniel, J.M., eds., Advances in the Study of Fractured Reservoirs: Geological Society of London, Special Publication 374, p. 79–95.

Schofield, K., and Adams, A.E., 1986, Burial dolomitization of the Woo Dale Limestones Formation (Lower Carboniferous), Derbyshire, England: Sedimentology, v. 33, p. 207–219.

Schultz, L.G., 1964, Quantitative interpretation of mineralogical composition from X-ray and chemical data for the Pierre Shale: U.S. Geological Survey, Professional Paper 391C, p. 1–31.

Sheppard, S.M.F., and Schwarcz, H.P., 1970, Fractionation of carbon and oxygen isotopes and magnesium between coexisting metamorphic calcite and dolomite: Contributions to Mineralogy and Petrology, v. 26, p. 161–198.

Shields, G., and Stille, P., 2001, Diagenetic constraints on the use of cerium anomalies as palaeoseawater redox proxies: an isotopic and ree study of Cambrian phosphorites: Chemical Geology, v. 175, p. 29–48.

Sibley, D.F., and Gregg, J.M., 1987, Classification of dolomite rock textures: Journal of Sedimentary Petrology, v. 57, p. 967–975.

Smith, E.G., Rhys., G.H., and Eden, R.A., 1967, The Geology of the country around Chesterfield, Matlock and Mansfield: British Geological Survey, Sheet 112.

Taylor, P., and Fryer, B., 1980, Multiple-stage hydrothermal alteration in porphyry copper systems in northern Turkey: the temporal interplay of potassic, propylitic, and phyllic fluids: Canadian Journal of Earth Sciences, v. 17, p. 901–926.

Tostevin, R., Shields, G., Tarbuck, G., He, T., Clarkson, M., and Wood, R., 2016, Effective use of cerium anomalies as a redox proxy in carbonate-dominated marine settings: Chemical Geology, v. 438, p. 146–162.

Vahrenkamp, V., and Swart, P., 1990, New distribution coefficient for the incorporation of strontium into dolomite and its implications for the formation of ancient dolomites: Geology, v. 18, p. 387–391.

Veizer, J., and Prokoph, A., 2015, Temperatures and oxygen isotopic composition of Phanerozoic Oceans: Earth Science Reviews, v. 146, p. 92–104.

Walkden, G.M., 1972, The mineralogy and origin of interbedded clay wayboards in the Lower Carboniferous of the Derbyshire Dome: Geological Journal, v. 8, p. 143–159.

Walkden, G.M., and Williams, D.O., 1991, The diagenesis of the Late Dinantian Derbyshire East Midland carbonate shelf, Central England: Sedimentology, v. 71, p. 643–670.

Walters, S.G., and Ineson, P.E., 1980, Mineralisation within the igneous rocks of the south Pennine orefiled: Peak District Mines Historical Society, Bulletin, v. 7, p. 315–325.

Webb, G.E., and Kamber, B.S., 2000, Rare earth elements in Holocene reefal microbialites: a new shallow seawater proxy: Geochimica et Cosmochimica Acta, v. 64, p. 1557–1565.

Webb, G.E., Nothdurft, L.D., Kamber, B.S., Kloprogge, J.T., and Zhao, J.-X., 2009, Rare earth element geochemistry of scleractinian coral skeleton during meteoric diagenesis: a sequence through neomorphism of aragonite to calcite: Sedimentology, v. 56, p. 1433–1463.

Whitaker, F., and Xiao, Y., 2010, Reactive transport modeling of early burial dolomitization of carbonate platforms by geothermal convection: American Association of Petroleum Geologists, Bulletin. v. 94, p. 889–917.

Wilson, A., Sanford W., Whitaker F., and Smart P., 2001, Spatial patterns of diagenesis during geothermal circulation in carbonate platforms: American Journal of Science, v. 301, p. 727–752.

Wood, D.A., Gibson, I., and Thompson, R.N., 1976, Elemental mobility during zeolite facies metamorphism of the Tertiary basalts of eastern Iceland: Contributions to Mineralogy and Petrology, v. 55, p. 241.

Zheng, Y.F., 1990, Carbon–oxygen isotopic covariation in hydrothermal calcite during degassing of CO_2: a quantitative evaluation and application to the Kushikino gold mining area in Japan: Mineralium Deposita, v. 25, p. 246–250.

Zheng, Y.F., and Hoefs, J., 1993, Carbon and oxygen isotopic covariations in hydrothermal calcites: theoretical modeling on mixing processes and application to Pb-Zn deposits in the Harz Mountains, Germany: Mineralium Deposita, v. 28, p. 79–89.

Received 28 October 2019; accepted 15 May 2020.